

# The $i_{11/2}f_{5/2}$ and $i_{11/2}p_{3/2}$ neutron particle-hole multiplets in $^{208}\text{Pb}$

A. Heusler

*Max-Planck-Institut für Kernphysik, D-69029 Heidelberg, Germany* \*

G. Graw, R. Hertenberger, F. Riess, and H.-F. Wirth<sup>†</sup>

*Sektion Physik der Universität München, D-85748 Garching, Germany* ‡

T. Faestermann and R. Krücken,

*Physik Department E12, Technische Universität München, D-85748 Garching, Germany*

J. Jolie, N. Pietralla, and P. von Brentano<sup>§</sup>

*Institut für Kernphysik, Universität zu Köln, D-50937 Köln, Germany*

Inelastic proton scattering via isobaric analog resonances allows to derive rather complete information about neutron particle-hole states. We applied this method to the doubly-magic nucleus  $^{208}\text{Pb}$  by measuring angular distributions of  $^{208}\text{Pb}(p, p')$  on top of the isobaric analog resonances in  $^{209}\text{Bi}$  with the Q3D magnetic spectrograph at München. We identify the six states of the  $i_{11/2}f_{5/2}$  multiplet and the four states of the  $i_{11/2}p_{3/2}$  multiplet in the energy range  $4.6 \text{ MeV} < E_x < 5.3 \text{ MeV}$ . Firm spin assignments for the ten states are given, some of them new. Additional measurements of the reaction  $^{207}\text{Pb}(d, p)$  confirm the fragmented  $i_{11/2}p_{1/2}$  multiplet.

PACS numbers: 21.10.-k, 21.10.Hw, 21.10.Jx, 21.60.-n, 21.60.Cs, 25.40.Ep, 25.40.Ny

## I. INTRODUCTION

$^{208}\text{Pb}$  is the heaviest easily accessible doubly magic nucleus. It is an ideal test laboratory to study the shell model in detail. For a wide range in excitation energy one-particle one-hole excitations are dominant, only at an excitation energy above  $E_x=5.3 \text{ MeV}$  four quasiparticle excitations resulting from collective two-phonon octupole modes [1, 2], start to contribute. The structure of the observed states is in agreement with theoretical expectations up to  $E_x=4.5 \text{ MeV}$  [2, 3, 4]. At higher energies, despite impressive experimental research [5, 6] not all states expected from the shell model have been detected. Many spin assignments are still ambiguous and in addition there are more states than expected in the 1-particle 1-hole frame.

Much information has been obtained by inelastically scattering protons via isobaric analog resonances (IAR-pp'). IAR-pp' is a selective reaction, sensitive to the neutron particle-hole components of the structure only. In this way the observed cross sections, its excitation functions and angular distributions, provide direct information on quantum numbers and amplitudes of the respective particle-hole configurations.

Early measurements of inelastic proton scattering via IAR [7, 8, 9, 10, 11, 12, 13, 14, 15] provided detailed information about the complex mixture of the neutron

particle-hole configurations. Since many years little work has been done in this field, we mention, however, the recent work done with the EUROBALL cluster detector [3]. The main reason is the need for an energy resolution of better than 5 keV in the spectra. At excitation energies  $E_x=4.2\text{-}4.8 \text{ MeV}$  in  $^{208}\text{Pb}$  there are a few doublets with a spacing below 10 keV. In the region  $E_x=5\text{-}6 \text{ MeV}$  the average distance of the known levels is already less than 10 keV. The work done in the 1960s by [12, 13, 14, 15] improved the energy resolution from 35 to 18 keV; some data were obtained using a magnetic spectrograph of 9-13 keV resolution [7, 14].

The present status of the Q3D facility at München [16, 17, 18, 19] allows to take (p, p') spectra with a resolution of about 3 keV within an energy span of around 1 MeV and high counting statistics on all known IAR in  $^{209}\text{Bi}$  and up to excitation energies of at least 8 MeV.

The IAR-pp' data are complemented by high statistics  $^{207}\text{Pb}(d, p)$  neutron transfer spectra, where the observed transfer quantum numbers are identical with the neutron particles coupled to the  $p_{1/2}$  hole configuration of the target  $^{207}\text{Pb}$  in its ground state.

In this paper we concentrate on the energy range  $E_x=4.5\text{-}5.3 \text{ MeV}$ , a region of considerable level density (at least 35 levels). We identify all members of the shell model configurations  $i_{11/2}f_{5/2}$  and  $i_{11/2}p_{3/2}$ . Because of the large value of the orbital angular momentum, the multiplet states based on the  $i_{11/2}$  neutron particle are weakly excited. It is one further step towards the goal of complete spectroscopy, as started in the early attempt [20] to derive "complete wave functions" and the residual interaction among 1-particle 1-hole particle-hole configurations from experimental data alone.

\*correspondance to: A.Heusler@mpi-hd.mpg.de

<sup>†</sup>now Physik Department E18, Technische Universität München, D-85748 Garching, Germany

<sup>‡</sup>supported by MLL and DFG C4-Gr894/2-3

<sup>§</sup>supported by DFG BR799/12-1

## II. SHELL MODEL

In order to describe the structure of the excited states in  $^{208}\text{Pb}$ , we restrict the shell model wave function to the 1-particle 1-hole configurations, neglecting 2-particle 2-hole and higher configurations. In the restricted shell model for  $^{208}\text{Pb}$  a state  $|\alpha I\rangle$  is described by a superposition of particle-hole configurations built from neutrons  $\nu$  and protons  $\pi$  relative to the  $0^+$  g.s. of  $^{208}\text{Pb}$ , see Fig. 1 for the neutron particle and hole configurations  $LJ, \nu$  and  $lj, \nu$ ,

$$|\alpha I\rangle = \sum_{LJ} \sum_{lj} c_{LJ,lj}^{\alpha I, \nu} |LJ, \nu\rangle \otimes |lj, \nu\rangle + \sum_{LJ} \sum_{lj} c_{LJ,lj}^{\alpha I, \pi} |LJ, \pi\rangle \otimes |lj, \pi\rangle. \quad (1)$$

Here we characterize a state  $|\alpha I\rangle$  by its spin (always given together with the parity),  $\alpha$  denoting the excitation energy  $E_x$  and other quantum numbers. The excitation energy is often given as a *label* by using [4] where known and omitting fractions of keV, *so an adopted value of the energy may differ by 1 keV*. If we restrict to this ansatz the amplitudes  $c_{LJ,lj}^{\alpha I, (\nu, \pi)}$  represent a unitary transformation of the shell model particle-hole configurations to the real states  $|\alpha I\rangle$ .

We introduce the short-hand writing  $|LJ, \nu\rangle$  for the neutron particle in the 6th shell with angular momentum  $L$  and spin  $J$  and similarly  $|lj, \nu\rangle$  for the neutron hole in the 5th shell,  $|LJ, \pi\rangle$  for the proton particle in the 5th shell,  $|lj, \pi\rangle$  for the proton hole in the 4th shell. We often omit the label  $\nu$  and simply write e.g.  $d_{5/2}$  since we will essentially only discuss neutron particle-hole configurations in this paper. From the context e.g. the meaning of the neutron particle  $|LJ, \nu\rangle = 6 d_{5/2}$  can be distinguished from the proton hole  $|lj, \pi\rangle = 4 d_{5/2}$ .

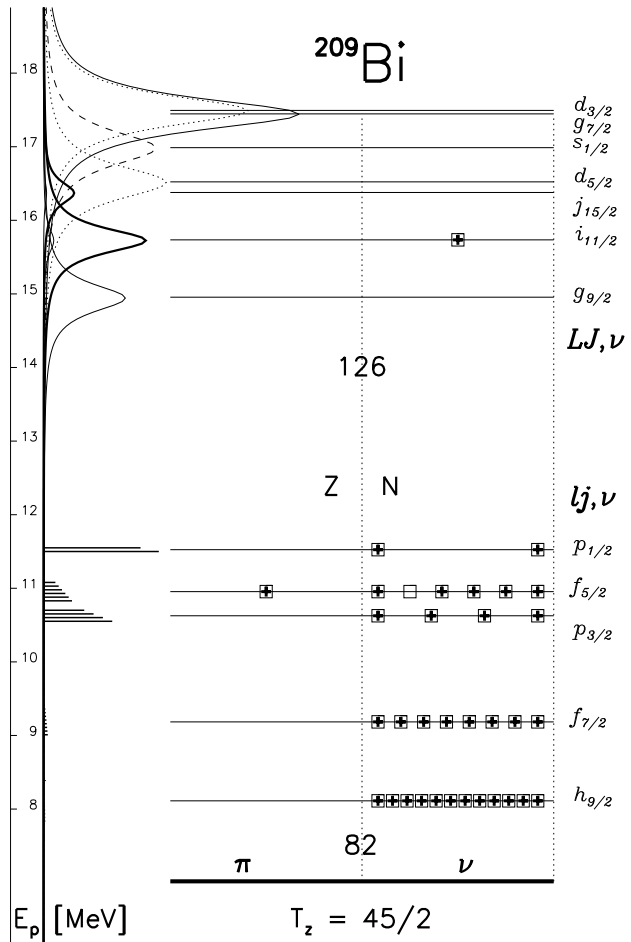
In the schematic shell model (SSM) the residual interaction is taken to be zero. The splitting of the multiplets in the full shell model depends on the strength of the diagonal and nondiagonal matrix elements of the residual interaction in  $^{208}\text{Pb}$  and of the relative separation of the undisturbed configurations in the SSM; matrix elements in the order of magnitude of some tens of keV are expected [20].

A rather pure structure will show up only in case of an isolated multiplet. Actually, however, the lowest 20 states in  $^{208}\text{Pb}$  ( $E_x < 4.5$  MeV) are heavily mixed since here the  $h_{9/2}s_{1/2}$  proton and the  $g_{9/2}f_{5/2}$  neutron configurations have almost the same SSM energy, and similarly the  $h_{9/2}d_{3/2}$  proton and the  $g_{9/2}p_{3/2}$ ,  $i_{11/2}p_{1/2}$  neutron configurations. An early attempt [20] determined the matrix elements of the effective residual interaction among particle-hole configurations in  $^{208}\text{Pb}$  from the configuration mixing in the lowest 20 states. However, some spin assignments and identifications of the states below  $E_x = 4.50$  MeV were essentially settled by the later work of [21]. In 1982, an update of the fit was done by one of us (A. H.); the results are shown in appendix A. There

is a remarkable agreement with shell model calculations by [22].

In contrast, the two multiplets built from the  $i_{11/2}$  neutron particle and the  $f_{5/2}$  and the  $p_{3/2}$  neutron hole, predicted at SSM energies  $E_x = 4.780$  and  $5.108$  MeV, respectively, are expected to be less mixed, at least for the high spin members ( $I = 5, 6, 7, 8$ ).

FIG. 1: Sketch of the IAR-pp' scenario for  $^{208}\text{Pb}(p, p')^{208}\text{Pb}^*$  (scale of proton energy  $E_p, E_{p'}$  at left). A single IAR state with spin  $LJ = i_{11/2}$  as the second member of the isobaric analog multiplet [ $^{209}\text{Pb}, ^{209}\text{Bi}, \dots$ ] is exemplified with *one* configuration  $i_{11/2}f_{5/2}$ , but all 45 excess neutrons  $lj, \nu$  including  $i_{11/2}$  participate equally, see Eq. 3. The excitation functions of all IAR are shown [12]; for the two weakest IAR  $i_{11/2}, j_{15/2}$  they are barely visible, therefore they are enhanced by a factor 10 (thick curves at left). The energies of the particle and hole configurations  $|LJ, \nu\rangle, |lj, \nu\rangle$  are taken from [6]. The penetrability of the Coulomb barrier can be estimated from the comparison of the maxima for the  $g_{9/2}, g_{7/2}$  (drawn) and the  $d_{5/2}, d_{3/2}$  (dotted) IAR. Similarly the penetrability of the outgoing particles  $lj, \nu$  can be seen from the comparison of the mean cross section for the particle-hole configurations  $|i_{11/2}, \nu\rangle \otimes |lj, \nu\rangle$  with spins  $I = J - j, \dots, j + j$  calculated from the s.p. widths derived by this work (lower left).



### III. SELECTIVE REACTIONS

Spectroscopic information about particle-hole configurations has been derived in addition to IAR-pp' from particle transfer reactions  $^{207}\text{Pb}(d, p)$ ,  $^{209}\text{Bi}(d, ^3\text{He})$ , and  $^{209}\text{Bi}(t, \alpha)$  [2, 4, 21] and from transitions due to the electromagnetic [3, 22] or the weak interaction [6]. IAR-pp' allows to identify the neutron components  $|LJ, \nu > \otimes |lj, \nu >$  of particle-hole states. The quantum number of the selected IAR is identical to the quantum number of the neutron particle configuration  $|LJ, \nu >$ , the angular distribution of the inelastically detected protons carry the information on the coherent contribution of the excess neutrons  $|lj, \nu >$ .

#### A. IAR-pp'

We discuss the inelastic proton scattering via isobaric analog resonances (IAR-pp') on a spin 0 target,  $|0^+ g.s. > \rightarrow \text{IAR}(LJ) \rightarrow |\alpha I >$ , here specifically  $^{208}\text{Pb}(p, p')$  proceeding via one of the lowest, well isolated IAR in  $^{209}\text{Bi}$ .

The wave function of an IAR in  $^{209}\text{Bi}$  with spin  $LJ$  may be represented by

$$|\Psi_{LJ}^{\text{IAR}}(^{209}\text{Bi}) > = \frac{1}{\sqrt{2T_0 + 1}} T_- |LJ, \nu > \otimes |^{208}\text{Pb}(0^+ g.s.) > \quad (2)$$

where  $T_0 = (N - Z)/2$  is the isospin of the g.s. of  $^{208}\text{Pb}$ . The isospin lowering operator  $T_-$  acts on all excess neutrons, hence we have

$$|\Psi_{LJ}^{\text{IAR}}(^{209}\text{Bi}) > = \frac{1}{\sqrt{2T_0 + 1}} |LJ, \pi > \otimes |^{208}\text{Pb}(0^+ g.s.) > + \sum_{lj} \sqrt{\frac{2j+1}{2T_0+1}} (|lj^{+1}, \pi > \otimes |lj^{-1}, \nu >)_{0^+} \otimes |LJ, \nu > \otimes |^{208}\text{Pb}(0^+ g.s.) >. \quad (3)$$

Evidently the outgoing proton either leaves  $^{208}\text{Pb}$  in its g.s. (elastic scattering) or creates a *neutron* particle-hole configuration  $|LJ, \nu > \otimes |lj, \nu >$  as shown in the sketch Fig. 1 for one specific example.

#### B. Angular distributions of $^{208}\text{Pb}(p, p')$

The IAR are described as Breit Wigner like resonance terms, their partial decay widths depend on the mixing coefficients  $c_{LJ, lj}^{\alpha I}$  and on penetrability effects. The resonance scattering is nicely described in the book of Bohr&Mottelson [23] in a general manner.

The differential cross section of the  $^{208}\text{Pb}(p, p')$  reaction on top of an isolated IAR ( $E_p = E_{LJ}^{\text{res}}$ ) proceeding to a state with neutron particle-hole configurations

$|LJ > \otimes |lj, \nu >$  is described [24] by

$$\frac{d\sigma_{LJ}^{\alpha I}}{d\Omega}(\Theta) = \frac{\hbar^2}{4\mu_0} \frac{(2I+1)}{(2J+1)} \frac{\Gamma_{LJ}^{s.p.}}{E_{LJ}^{\text{res}} (\Gamma_{LJ}^{\text{tot}})^2} \times \sum_{lj} \sum_{l'j'} a_{LJ, lj, l'j'}^{IK} P_K(\cos(\Theta)) c_{LJ, lj}^{\alpha I} \sqrt{\Gamma_{lj}^{s.p.}} \cos(\xi_{lj}^{s.p.} - \xi_{l'j'}^{s.p.}) c_{LJ, l'j'}^{\alpha I} \sqrt{\Gamma_{l'j'}^{s.p.}} \quad (4)$$

where  $\xi_{lj}^{s.p.}$  are phases derived from theory [25] and  $\mu_0 = m(p)m(^{208}\text{Pb})/(m(p) + m(^{208}\text{Pb}))$  is the reduced mass. The factors  $a_{LJ, lj, l'j'}^{IK}$  arise from the recoupling of the angular momenta  $L, l$  and spins  $J, j$  to  $I, K$

$$a_{LJ, lj, l'j'}^{IK} = (-)^{(I+2J)} W(jJj'J, IK) \times \bar{Z}(LJLJ, \frac{1}{2}K) \bar{Z}(lj'l'j', \frac{1}{2}K), \quad (5)$$

where  $K \leq \min(2L, 2J, \max(2l), \max(2j))$  is even; the recoupling coefficients  $W, \bar{Z}$  are defined by [26, 27], see appendix B.

The component with  $K = 0$  represents the mean cross section  $\sigma_{LJ}^{\alpha I}$ ; for a state  $|\alpha I >$  it is just the sum of the configuration strength  $|c_{LJ, lj}^{\alpha I}|^2$  weighted by the s.p. widths,

$$\sigma_{LJ}^{\alpha I} = \frac{\hbar^2}{4\mu_0 E_{LJ}^{\text{res}}} \frac{(2I+1)}{(2J+1)} \frac{\Gamma_{LJ}^{s.p.}}{(\Gamma_{LJ}^{\text{tot}})^2} \sum_{lj} |c_{LJ, lj}^{\alpha I}|^2 \sqrt{\Gamma_{lj}^{s.p.}}^2. \quad (6)$$

For a multiplet of states  $|\alpha I >$  with spins  $I = J - j, \dots, J + j$  consisting mainly of one configuration  $|LJ > \otimes |lj >$ , the angle averaged (mean) cross sections  $\sigma_{LJ}^{\alpha I}$  on top of a specific IAR  $LJ$  should be simply related to the spin factor  $2I + 1$ , neglecting contributions from other IAR.

In general several configurations are to be considered; the formula describing the angular distribution of the IAR-pp' reaction (Eq. 4) comprises a sum of products for coherent amplitudes  $c_{LJ, lj}^{\alpha I}$ . Hence the relative phases of the amplitudes can be determined.

Each pure neutron particle-hole configuration  $|(LJ, \nu > \otimes |lj, \nu >)_I >$  has a characteristic angular distribution  $\sum_K a_K P_K(\Theta)$  of even Legendre polynomials (appendix B). Small admixtures of other neutron particle-hole configurations sometimes change the values  $a_K$  considerably, however.

The highest spin of each configuration  $|LJ > \otimes |lj >$  produce a deep minimum of the angular distribution at  $90^\circ$ , which is the more pronounced the higher the angular momenta  $LJ, lj$  are. Similarly, for the lowest spin a deep minimum of the angular distribution at  $90^\circ$  is found. This gives the chance to assign spins in certain cases rather firmly.

Unfortunately we could not measure at scattering angles beyond  $115^\circ$  for technical reasons. IAR-pp' angular distributions should be symmetric around  $90^\circ$  in the absence of direct-(p, p') contributions. Hence an angular distribution rising towards forward angles sometimes is difficult to interpret.

In case a group of states represents a rather complete subset of particle-hole configurations, the coefficients  $c_{LJ,lj}^{\alpha I,(\pi,\nu)}$  of the unitary transformation matrix may be determined from the analysis of IAR-pp' together with the observation of the ortho-normality rule and the sum-rule relations. Often there are less free parameters to be fitted than the IAR-pp' data provides. So in principle, amplitudes of proton particle-hole configurations can be determined [20].

Crucial for such an analysis is the correct identification of all relevant states and firm spin and parity assignments.

TABLE I: Parameters for IAR in  $^{209}\text{Bi}$ . For some IAR  $LJ$  and some outgoing waves  $lj$  new values are derived (right-most column), see appendix C. The energy dependence of the penetrability for the escape widths  $\Gamma_{LJ}^{s.p.}$  can be globally approximated by Eq. 10 in the region  $10\text{ MeV} < E_{p'} < 12\text{ MeV}$ .

$LJ$	$E_{LJ}^{res}$ MeV [12]	$\Gamma_{LJ}^{tot}$ keV [12]	$\Gamma_{LJ}^{s.p.}$ keV [12]	$R_{LJ}$ [12]	$\Gamma_{LJ}^{s.p.}$ keV
$g_{9/2}$	$14.918 \pm 0.006$	$253 \pm 10$	$20 \pm 1$	8	
$i_{11/2}$	$15.716 \pm 0.010$	$224 \pm 20$	$2 \pm 0.8$	1	$2.2 \pm 0.3$
$j_{15/2}$	$16.336 \pm 0.015$	$201 \pm 25$		$0.4^a$	$0.7 \pm 0.3^a$
$d_{5/2}$	$16.496 \pm 0.008$	$308 \pm 8$	$45 \pm 5$	12	
$s_{1/2}$	$16.965 \pm 0.014$	$319 \pm 15$	$45 \pm 8$	11	
$d_{3/2}$	$17.430 \pm 0.010$	$288 \pm 20$	$35 \pm 10$	$(20)^b$	
$g_{7/2}$	$17.476 \pm 0.010$	$279 \pm 20$	$45 \pm 10$	$(20)^b$	
$lj$	$E_{lj}^{p'}$ MeV [14] <sup>c</sup>		$\Gamma_{lj}^{s.p.}$ keV [14]		$\Gamma_{lj}^{s.p.}$ keV
$p_{1/2}$	11.49		$28.6 \pm 3$		$28.6^d$
$f_{5/2}$	10.92		$4.2 \pm 0.4$		$5.2 \pm 0.4$
$p_{3/2}$	10.59		$15.8 \pm 1.5$		$14.6 \pm 0.5$
$f_{7/2}$	9.15		0.6		$0.55 \pm 0.1^e$

<sup>a</sup>from a preliminary analysis of the 4610, 4860, 4867 states with spins  $8^+, 8^+, 7^+$

<sup>b</sup>doublet IAR, definition of  $R_{LJ}$  valid for isolated IAR only

<sup>c</sup> $E_{lj}^{p'} = E_{LJ}^{res} - E_{LJ,lj}^{SSM}$  corresponds to the SSM energy of the particle-hole configuration  $|LJ > \otimes |lj >$ , see Fig. 1.

<sup>d</sup>This value was not adjusted since the systematic errors of the absolute cross section are about 10-20%. They can be reduced by a more complete evaluation of our IAR-pp' data [28].

<sup>e</sup>from a preliminary analysis of the 5935 state identified to contain most of the  $g_{9/2}f_{7/2} 8^-$  configuration

### C. Energy dependence of the s.p. widths

The s.p. widths strongly depend on the angular momentum  $L$  of the IAR since the outgoing particle has to penetrate the Coulomb barrier. Fig. 1 gives an impression about the relative values of the penetrability. The  $i_{11/2}$  IAR with  $l = 4$  has the weakest penetrability of all positive parity IAR we measured.

We define a penetrability ratio

$$R_{LJ} = \frac{\Gamma_{LJ}^{s.p.}/(\Gamma_{LJ}^{tot})^2}{\Gamma_{i_{11/2}}^{s.p.}/(\Gamma_{i_{11/2}}^{tot})^2}; \quad (7)$$

it compares the cross section on some IAR  $LJ$  to that on the  $i_{11/2}$  IAR. In fact it essentially takes care of the different penetrability of the particle populating each IAR. Using the data and analysis of [12, 14] we derive values  $R_{LJ}=8, 12, 11$  for  $LJ=g_{9/2}, d_{5/2}, s_{1/2}$  IAR, respectively, see Tab. I. For the doublet  $d_{3/2}+g_{7/2}$  IAR we assume a factor 20, but we note that the given equations are valid for isolated IAR [29, 30] only.

### D. Overlapping IAR

Eqs. 4, 6 are valid for isolated IAR only. The lowest IAR in  $^{209}\text{Bi}$  are well isolated, but the  $i_{11/2}$  IAR is rather weak as can be seen in Fig. 1 where it is enhanced by a factor 10 in order to make it visible at all. Hence the tails from neighbouring  $g_{9/2}$  and  $d_{5/2}$  IAR may interfere with the  $i_{11/2}$  IAR. (The penetrability ratio is  $R_{g_{9/2}}, R_{d_{5/2}}=8, 12$ .) Following the formula for excitation functions given by [12], the  $g_{9/2}, d_{5/2}$  IAR have decayed by a factor 40, 25, respectively, from the top of the IAR ( $E_p=14.920, 16.945\text{ MeV}$ , respectively) to  $E_p=15.720\text{ MeV}$ , the resonance energy of the  $i_{11/2}$  IAR. Since in IAR-pp' the amplitudes are relevant, the population on top of the  $i_{11/2}$  IAR by the neighbouring IAR can be still considerable. However, the influence of the  $g_{9/2}$  IAR may be neglected since the relative amplitude is only of the order of 15%, while for the  $d_{5/2}$  IAR the relative amplitude is still about 50%.

Yet for the  $i_{11/2}f_{5/2}, i_{11/2}p_{3/2}$  multiplets being considered, this problem does not apply since there must be an allowed entrance channel. For the higher spins only the configurations  $d_{5/2}h_{9/2}, d_{5/2}h_{11/2}$  may contribute, but the penetrability of the outgoing  $l = 5$  particle is 10 and 50 times lower than for  $f_{5/2}$  and  $p_{3/2}$ , respectively. In addition any contribution of these configurations is expected to be small. Only for a  $3^-$  state the entrance channel  $d_{5/2}p_{1/2}$  may contribute eventually.

We conclude that IAR-pp' is a method able to detect and analyze even weakly excited neutron particle-hole states.

## IV. EXPERIMENTS

We performed experiments on  $^{208}\text{Pb}(p, p')$  and  $^{207}\text{Pb}(d, p)$ . The high Q-value of the reaction  $^{209}\text{Bi}(d, ^3\text{He})$  prohibited any reasonable experiment with the Q3D facility due to the restricted energy range of the accelerator.

The data are evaluated by help of the computer code GASPAN [31]. It allows the deconvolution of spectra into a set of peaks with gaussian shape of individual widths and exponential tails on a background with polynomial shape. The energy calibration takes care of the quadratic dependence on the channel due to the effect of the magnetic field.

TABLE II: Parameters for the  $^{208}\text{Pb}(p, p')$  experiment. Targets enriched in  $^{208}\text{Pb}$  to 99.85% were used. The thickness of the targets T2, T3, T4 were 98, 245, 353  $\mu\text{g}/\text{cm}^2$ ; the thickness of target T1 was determined as 104  $\mu\text{g}/\text{cm}^2$  by comparison to other targets.

IAR	$E_p$ [MeV]	$E_x$ [MeV]	$\Theta$	targets	# runs
$g_{9/2}$	14.920	3.85 - 6.2	$48^\circ - 115^\circ$	T1 - T4	57 <sup>a b</sup>
$i_{11/2}$	15.720	4.05 - 5.85	$20^\circ - 115^\circ$	T1 - T3	44 <sup>c d</sup>
$j_{15/2}$	16.355 <sup>e</sup>	4.55 - 6.0	$66^\circ - 115^\circ$	T2 - T3	22
$d_{5/2}$	16.495	3.73 - 6.9	$36^\circ - 115^\circ$	T1 - T4	39 <sup>f g</sup>
$s_{1/2}$	16.960	5.00 - 6.9	$48^\circ - 115^\circ$	T2 - T4	12 <sup>h i</sup>
$d_{3/2}+g_{7/2}$	17.480 <sup>j</sup>	5.54 - 6.8	$84^\circ, 115^\circ$	T2 - T3	12 <sup>k l</sup>

<sup>a</sup>2 runs at  $\Theta = 54^\circ, 90^\circ$  covering  $E_x=2.1-3.85$  MeV

<sup>b</sup>1 run at  $\Theta = 58^\circ$  covering  $E_x=6.2-6.65$  MeV

<sup>c</sup>3 runs at  $\Theta = 105^\circ, 115^\circ$  covering  $E_x=3.85 - 4.05$  MeV,

<sup>d</sup>1 run at  $\Theta = 105^\circ$  covering  $E_x=5.85 - 6.18$  MeV

<sup>e</sup>in addition 16.290, 16.380, 16.290

<sup>f</sup>1 run at  $\Theta = 48^\circ$  covering  $E_x=3.65 - 3.73$  MeV

<sup>g</sup>3 runs at  $\Theta = 48^\circ, 84^\circ$  covering  $E_x=6.9 - 7.4$  MeV

<sup>h</sup>1 run at  $\Theta = 84^\circ$  for  $E_x=3.65 - 5.0$  MeV

<sup>i</sup>1 run at  $\Theta = 115^\circ$  for  $E_x=6.9 - 7.2$  MeV

<sup>j</sup>in addition 17.590, 17.610, 17.720

<sup>k</sup>2 runs at  $\Theta = 84^\circ$  covering  $E_x=4.7 - 5.54$  MeV

<sup>l</sup>2 runs at  $\Theta = 84^\circ$  covering  $E_x=6.8 - 7.2$  MeV

TABLE III: Parameters for the  $^{208}\text{Pb}(d, p)$  experiment with the Q3D facility. The deuteron energy was  $E_d=22.000$  MeV as for [2]. A target enriched in  $^{207}\text{Pb}$  to  $99.86\pm.04\%$  was used. The slits perpendicular to the scattering angle were kept open,  $\Delta\Phi = \pm 3^\circ$ .

$E_x$ [MeV]	scattering angle $\Theta$	slit opening $\Delta\Theta$	# runs
3.5 - 5.2	$20^\circ$	$\pm 0.9^\circ$	1
3.1 - 7.9	$20^\circ$	$\pm 1.5^\circ$	3
3.1 - 5.5	$25^\circ$	$\pm 0.9^\circ$	3
3.1 - 7.9	$25^\circ$	$\pm 1.5^\circ$	3
3.1 - 5.1	$30^\circ$	$\pm 0.6^\circ$	1
3.1 - 5.2	$30^\circ$	$\pm 0.9^\circ$	1
5.7 - 8.0	$30^\circ$	$\pm 0.9^\circ$	2
3.1 - 8.0	$30^\circ$	$\pm 1.5^\circ$	6

Here we report on results leading to the detection of the main components of the  $i_{11/2}f_{5/2}$  and the  $i_{11/2}p_{3/2}$  multiplets in  $^{208}\text{Pb}$ . Other data are being evaluated; the raw data (together with excerpts from the runbook) can be accessed [28].

A preliminary analysis is in agreement with data from ref. [7, 8, 9, 10, 11, 12, 13, 14, 15] obtained in the 1960s. Of course, because of the much higher resolution many levels are resolved to be doublets. An important difference is the better energy calibration, their energies deviate linearly by about 5-10 keV for the range 4-6 MeV; mostly the energies are about 0.2% too low.

### A. $^{208}\text{Pb}(p, p')$ experiment with the Q3D facility

The  $^{208}\text{Pb}(p, p')$  experiment was performed with a proton beam from the München HVEC MP Tandem accel-

erator using the Q3D magnetic spectrograph. The bright Stern-Gerlach polarized ion source was used with unpolarized hydrogen [16, 19]. At beam intensities of about 900 nA, the target was wobbling with a frequency of 2 sec to avoid damage of the lead target. The proton energies were chosen according to [12] to match the top of the seven lowest IAR in  $^{209}\text{Bi}$ , namely the  $g_{9/2}$ ,  $i_{11/2}$ ,  $j_{15/2}$ ,  $d_{5/2}$ ,  $s_{1/2}$  IAR and the doublet-IAR  $g_{7/2}+d_{3/2}$ ; some more energies slightly off-resonance were chosen, see Tab. II. The analyzed particles were detected in an ASIC supported cathode strip detector [17, 18]. At an active length of 890 mm it produces spectra where the position of a line is determined to better than 0.1 mm without systematic errors. With a few exceptions the slits of the magnetic spectrograph were kept open,  $\Delta\Theta = \pm 3^\circ$ ,  $\Delta\phi = \pm 3^\circ$ .

### B. Experiments on $^{207}\text{Pb}(d, p)$

A weak excitation by  $^{207}\text{Pb}(d, p)$  may help to decide some spin and configuration assignments. Therefore, we measured the reaction  $^{207}\text{Pb}(d, p)$  with the goal to detect as low spectroscopic factors (S.F.) as possible. We performed two measurements, one with the (gone) Buechner spectrograph at Heidelberg at large backward angle in order to eliminate any contamination from light nuclei in the spectrum, another experiment with the Q3D facility at München where the deuteron energy was chosen to match [2].

(a) *Buechner spectrograph*. In 1969, using the Heidelberg Tandem van de Graaff accelerator, two of us (A. H., P. von B.) did a deep exposure of  $^{207}\text{Pb}(d, p)$  with the Buechner magnetic spectrograph gathering 6 mCb of the deuteron beam in more than 30 hours. The scattering angle was chosen as  $\Theta = 130^\circ$ . The target was enriched to 92%. A short exposure was done to position the line from the 3.708 MeV  $5^-$  state properly. The energy range was  $3.65 \text{ MeV} < E_x < 5.15 \text{ MeV}$ . This data was crucial for the fit shown in [20] and now is still useful albeit the resolution of only 12 keV. It has been reevaluated by use of the GASPAN code [31].

(b) *Q3D spectrograph*. The study of the reaction  $^{207}\text{Pb}(d, p)$  was performed with a deuteron beam from the München HVEC MP Tandem accelerator. The high performance of the Q3D facility allowed to take 18 spectra with superior resolution during 30 hours with beam intensities of about 600 nA. Tab. III shows the parameters relevant to the data taking.

In order to detect even minor contaminations (e.g. from  $^{23}\text{Na}$ ,  $^{35}\text{Cl}$ ,  $^{37}\text{Cl}$ ) we measured at scattering angles  $\Theta = 20^\circ, 25^\circ, 30^\circ$  with different slit openings, see Tab. III. We achieved a peak-to-valley ratio of better than  $1 : 10^{-4}$  which allows the detection of S.F. as low as a few  $10^{-3}$  in favorable cases. By this means, the amount of the impurity isotopes  $^{206}\text{Pb}$ ,  $^{208}\text{Pb}$  could be measured as  $0.028\pm.003\%$ ,  $0.11\pm.03\%$ , respectively.

The 5292, 4610 keV levels in  $^{208}\text{Pb}$  (Tab. IV, V) are

known to be populated by a  $l = 0, l = 5$  transfer, respectively. The measurement at three scattering angles allows to discriminate the transfer of a  $l = 0, l = 5$  neutron by virtue of a steeply rising slope for the angular distribution. This gives a chance to determine the  $l$ -value for some levels. Other  $l$ -values have about equal cross sections for  $\Theta = 20^\circ, 25^\circ, 30^\circ$ .

FIG. 2: Spectra of  $^{208}\text{Pb}(p, p')$  for  $E_x=4.6$ -5.0 MeV taken at  $\Theta = 58^\circ, 72^\circ, 54^\circ$  on the  $g_{9/2}$ ,  $i_{11/2}$ ,  $d_{5/2}$ , with targets T3, T2, T2 (see caption of Tab. II), respectively. Six levels resonate at  $E_p=15.72$  MeV on top of the  $i_{11/2}$  IAR (black fill out); the doublet at 4709, 4711 keV is resolved by the computer code GASPAN only. The energies of the  $i_{11/2}f_{5/2}$  multiplet are given in the middle panel and shown by bars above and below; in the lower panel the spins are given, too. The counting interval is proportional to  $\sqrt{E_x}$  and one step corresponds to about 0.3 keV.

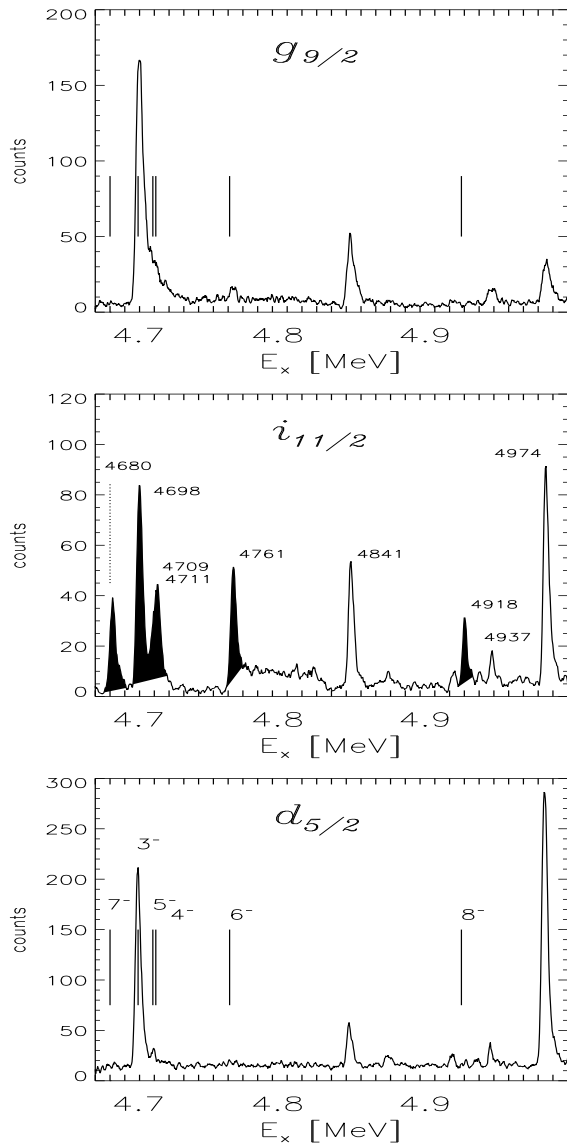
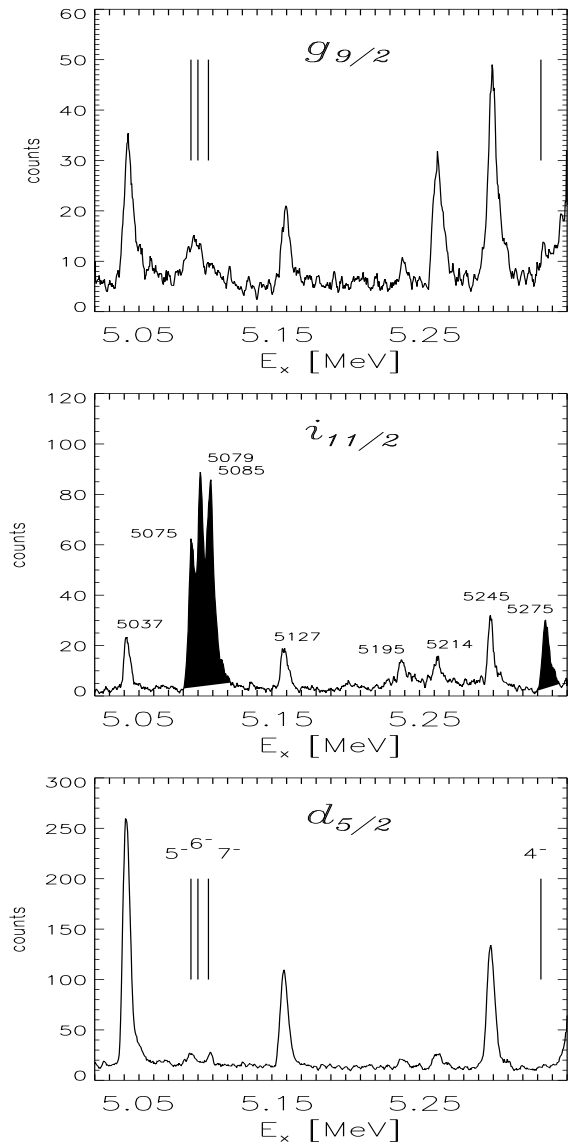


FIG. 3: Spectra of  $^{208}\text{Pb}(p, p')$  for the  $i_{11/2}p_{3/2}$  multiplet in the region  $E_x=5.0$ -5.3 MeV. The energies of the multiplet are given in the middle panel, the spins in the lower panel. For other details refer to Fig. 2 and the text.



### C. Typical spectra for $^{208}\text{Pb}(p, p')$

In Fig. 2, 3 we show some spectra for  $^{208}\text{Pb}(p, p')$  taken on the  $i_{11/2}$  IAR. For comparison spectra taken on the  $g_{9/2}$ ,  $d_{5/2}$  IAR are displayed, too. In total we measured nearly 200 spectra. We will discuss the excitation of the levels at  $E_x=4680, 4698, 4761, 4918, 5275$  keV and the clearly resolved multiplet at  $E_x=5075, 5079, 5085$  keV (black fill-out in the spectra taken on the  $i_{11/2}$  IAR, bars on the other IAR).

The 4709, 4711 doublet is resolved by help of the computer code GASPAN [31]; the distance is found to be 1.9 keV with an average resolution of somewhat less than 3.0 keV FWHM for spectra, see Fig. 2. The line contents

TABLE IV: Energies for levels excited by  $^{208}\text{Pb}(p, p')$  but *not* bearing the main strength of the configurations  $i_{11/2}f_{5/2}$ ,  $i_{11/2}p_{3/2}$ . Not all of them are also detected by the  $^{207}\text{Pb}(d, p)$  experiment. The energies from  $^{208}\text{Pb}(p, p')$  are not yet finally evaluated, therefore they are just given as a label with a precision of around 1 keV. The dominant excitations by specific IAR are shown; for strong excitations the energy label is printed **boldface**, for weak excitations an important IAR is given in parentheses. Energies and mean cross sections  $\sigma_{LJ}^{\alpha I}$  ( $\Theta = 20^\circ, 25^\circ, 30^\circ$ ) derived from  $^{207}\text{Pb}(d, p)$  are shown. Spins from [4] and energies from [2, 3, 4] are given for comparison.

$E_x$ (p, p')	main IAR	$E_x$ keV (d, p)	$\sigma(25^\circ)$ $\mu\text{b}/\text{sr}$ (d, p)	$E_x$ keV [4]	$E_x$ keV [2]	$E_x$ keV [3]	spin [4]
<b>5292</b>	$s_{1/2}$	5292.1	637	5292.000	5292.6	5292.7	$1^-$
		0.2		0.200	1.5	0.1	
5280	$s_{1/2}$	5280.3	210	5280.322	5281.3	5280.3	$0^-$
		0.2		0.080	1.5	0.1	
<b>5245</b>	$d_{5/2}$	5245.3	713	5245.280	5245.6	5245.4	$3^-$
		0.2		0.060	1.5	0.1	
5239	$(i_{11/2})$	5239.5	10	5239.350	5240.8	–	$0^+$
		0.7		0.360	1.5	–	
5214	$d_{5/2}$	5214.0	45	5213.000	5215.6	–	$6^+$
		0.3		0.200	1.5	–	
5195	$j_{15/2}$	5195.0	17	5195.340	5194.3	–	$7^+$
		0.3		0.140	0.6	–	
5194	$j_{15/2}$	–	< 5	5193.400	–	–	$5^+$
				0.150	–	–	
<b>5127</b>	$d_{5/2}$	5127.4	682	5127.420	5127.1	–	$2, 3^-$
		0.3		0.090	0.6	–	
5105	$(i_{11/2})$	–	< 5	–	5103.3	–	
					1.5	–	
5093	$j_{15/2}$	5093.2	14	5093.110	5094.3	–	$8^+$
		0.5		0.200	1.5	–	
5069	$d_{5/2}$	–	< 5	5069.380	5068.5	–	$10^+$
				0.130	1.5	–	
5037	$d_{5/2}$	5037.4	1200	5037.520	5037.2	5037.0	$2^-$
		0.2		0.050	0.6	0.1	
5010.5	$(j_{15/2})$	–	< 5	5010.550	5010.0	–	$9^+$
				0.090	0.6	–	

could be measured quite well using a special option of GASPAN (fixed level distances) yielding usable angular distributions.

Some excitations belong to well known levels (Tab. IV, V). A few weak lines are also clearly identified, among them are the  $0^+$  state at 5239 keV identified by [1] to have the 2-particle 2-hole structure  $|2614 \text{ keV } 3^- \otimes |2614 \text{ keV } 3^- \rangle$ , the  $0^-$  state at 5280 keV separated from the 5276 keV  $8^-$  state by only 4 keV, the 4860, 4867 keV doublet with spins  $8^+$ ,  $7^+$  strongly excited on the  $j_{15/2}$  IAR.

For the shown spectra (Fig. 2, 3) only a few contamination lines are present; prominent contamination lines start at  $E_x \approx 5.29 \text{ MeV}$  for the spectra taken both on the  $g_{9/2}$  and the  $d_{5/2}$  IAR. A weak contamination line is visible in the region 4.76-4.82 MeV on the  $i_{11/2}$  IAR, kinematically broadened.

Most levels in discussion are excited strongest on the

TABLE V: ... continuing Tab. IV

$E_x$ (p, p')	main IAR	$E_x$ keV (d, p)	$\sigma(25^\circ)$ $\mu\text{b}/\text{sr}$ (d, p)	$E_x$ keV [4]	$E_x$ keV [2]	$E_x$ keV [3]	spin [4]
4992	$(j_{15/2})$	4992.5	10	–	4992.7	–	
		0.6			0.6	–	
<b>4974</b>	$d_{5/2}$	4973.9	1350	4974.037	4974.2	4973.8	$3^-$
		0.2		0.040	0.6	0.1	
4953	$(d_{5/2})$	–	< 5	4953.320	4952.2	–	$3^-$
				0.230	0.3	–	
4937	$d_{5/2}$	4937.4	33	4937.550	4937.1	4935.1	$3^-$
		0.4		0.230	0.3	0.2	
4928	$(j_{15/2})$	–	< 5	–	4928.1	–	
					1.5	–	
4911	$(d_{5/2})$	4911.7	6	–	4910.6	–	
		0.5			1.5	–	
4909	$(j_{15/2})$	–	< 5	–	–	–	
4895	$j_{15/2}$	–	< 5	4895.277	4894.8	–	$10^+$
				0.080	1.5	–	
4867	$j_{15/2}$	4868.1	95	4867.816	4866.9	–	$7^+$
		0.2		0.080	1.5	–	
4860	$j_{15/2}$	4860.8	35	4860.840	4859.8	–	$8^+$
		0.3		0.080	1.5	–	
4841	$d_{5/2}$	4841.7	22	4841.400	4841.7	4842.1	$1^-$
		0.4		0.100	0.3	0.1	
4610	$j_{15/2}$	4610.7	66	4610.795	4610.8	4610.5	$8^+$
		0.3		0.070	0.5	0.3	

$i_{11/2}$  IAR, the only exception is the 4698 keV  $3^-$  state. On the  $i_{11/2}$  IAR, the levels at 4680, 4761, 4918, 5079 keV are at least four times stronger excited than on any other IAR.

## V. DATA ANALYSIS

### A. Excitation energies from $^{208}\text{Pb}(p, p')$

In Tab. VI we show the excitation energies derived from our measurements of  $^{208}\text{Pb}(p, p')$ . The spectra were calibrated by using around 40 reference energies below  $E_x=6.0 \text{ MeV}$  and about 25 more reference energies up to  $E_x=7.5 \text{ MeV}$  mainly from [4], but also from [2, 3]; see Tab. IV, V for the region of interest.

We avoided the usage of reference values in cases where the identification due to a multiplet structure was unclear or where the cross section was low. In addition to the quadratic dependence of the energy from the channel in the Q3D spectra, a secondary fit by a third order parabola improved the energy calibration considerably, see [32].

The excitation energies determined from the IAR-pp' measurement with errors of about 0.5 keV in general, compare well to [2, 3, 4] within the given errors; the only exception is the 5075 level with a discrepancy of about two standard errors.

## B. Excitation functions of $^{208}\text{Pb}(\text{p}, \text{p}')$

With a few exceptions, we did not measure excitation functions, but selected the energies of all known IAR only, see Tab. II. IAR often excite the states rather selectively. So we can determine excitation functions in a schematic manner. For some levels excitation functions were measured in the 1960s [12, 13]. We will mention them in place.

The angular distributions were fitted by even Legendre polynomials

$$\frac{d\sigma_{LJ}^{\alpha I}}{d\Omega}(\Theta) = \sum_K A_K P_K(\cos(\Theta)) \quad (8)$$

Odd Legendre polynomials have not to be included since the direct-(p, p') reaction does not contribute much in most cases. The angle averaged (mean) cross section is derived for each IAR  $LJ$  and each state  $|\alpha I\rangle$  as  $\sigma_{LJ}^{\alpha I} = A_0$ . We don't quote neither the errors of  $\sigma_{LJ}^{\alpha I}$  nor the values  $A_K$  for  $K > 0$  since the evaluation can be further improved. The errors of the mean cross sections are about 5-20%.

In Fig. 4 we show the excitation functions in a schematic manner. For each of the ten states in discussion and for each IAR the mean cross section  $\sigma_{LJ}^{\alpha I}$  is shown. All levels in discussion show a pronounced excitation by the  $i_{11/2}$  IAR. They have weak counterparts on all other IAR.

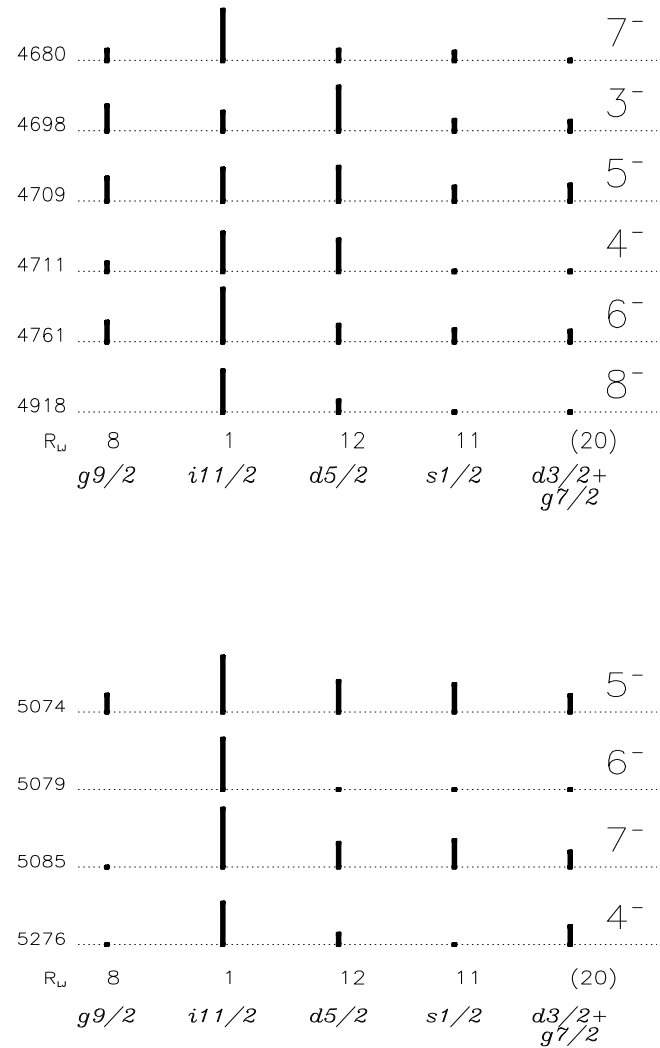
In reality due to the low penetrability of the  $i_{11/2}$  particle, the cross sections for the  $g_{9/2}$ ,  $d_{5/2}$ ,  $s_{1/2}$  IAR must be reduced by the penetrability ratio  $R_{LJ}=8, 12, 11, (20)$  (Eq. 7 and Tab. I) in relation to the  $i_{11/2}$  IAR, see Tab. VI. Taking into account these values, Fig. 4 demonstrates that the ten states are rather pure.

## C. Angular distributions of $^{208}\text{Pb}(\text{p}, \text{p}')$

In Fig. 5, 6 and 7 we show the angular distributions for some members of the  $i_{11/2}f_{5/2}$  multiplet and all members of the  $i_{11/2}p_{3/2}$  multiplet. The cross sections are shown on a logarithmic scale in  $\mu\text{b}/\text{sr}$ ; the scale of the scattering angles is  $0^\circ < \Theta < 120^\circ$ , the highest angle where we could measure was  $115^\circ$ ; below  $20^\circ$  the spectra became unusable due to increasing slit scattering. The spin assignment is discussed below.

Calculations for the pure particle-hole configurations by Eq. 4 are inserted for the angular distributions (dotted line) and the angle averaged (mean) cross section  $\sigma_{LJ}^{\alpha I}$  (dashed line). The absolute value of the calculated angular distributions has been adjusted to an approximate best-fit for the  $8^-$  state of the  $i_{11/2}f_{5/2}$  group and for the  $7^-$  state of the  $i_{11/2}p_{3/2}$  group yielding a more precise value of  $\Gamma_{i_{11/2}}^{s.p.}$ . For the states with other spins no adjustment has been done except for the energy dependence of the penetrability (Eq. 9, 10).

FIG. 4: Angle averaged (mean) cross section  $\sigma_{LJ}^{\alpha I}$  for states containing most of the  $i_{11/2}f_{5/2}$  strength (*upper panel*) and  $i_{11/2}p_{3/2}$  strength (*lower panel*). The value  $\sigma_{LJ}^{\alpha I}$  for each state is shown relative to the maximum of all cross sections of either multiplet; the maxima are set equal (upper panel: 4761  $6^-$ , lower panel: 5085  $7^-$ , see tab VI). At the left and right side the energy labels and the spins are given. In order to obtain partial widths (Eq. 6), for each IAR  $LJ$  the mean cross section must be reduced by the penetrability ratio  $R_{LJ}$  given at bottom.



For the  $i_{11/2}p_{3/2}$  group there is a general agreement of the mean cross section with the calculation, whereas for the  $i_{11/2}f_{5/2}$  group only the states with highest spins  $7^-$ ,  $8^-$  agree with the expectation of a rather pure configuration. The 4698 level has a cross section about ten times higher than expected. For the  $4^-$ ,  $6^-$  states the shape of the angular distributions agrees with the



expectation of a rather pure configuration, but the angle averaged (mean) cross section is around 50% higher. For the  $5^-$  state the angular distribution (*not shown*) deviates from a  $i_{11/2}f_{5/2}$  distribution at forward angles  $\Theta < 60^\circ$  up to a factor 4.

Note that the angular distribution of the members with the highest spin  $I = J + j$  for the configurations  $i_{11/2}p_{3/2}$  and  $i_{11/2}f_{5/2}$  (Fig. 3: 5085  $7^-$ , Fig. 2: 4918  $8^-$ ) are similar, both show the characteristic minimum at  $\Theta = 90^\circ$ . As expected for the lowest spin  $I = J - j$ , the 5276  $4^-$  state (Fig. 3) exhibits the characteristic forward peaking similar as for the highest spin  $I = J + j$ .

FIG. 5: Angular distributions for the 4.71 MeV doublet partner with spin  $4^-$  and the state with spin  $6^-$ . The mean cross section for a pure configuration  $i_{11/2}f_{5/2}$  calculated by Eq. 6 is shown by a dashed line; the corresponding angular distributions calculated by Eq. 4 is shown by the dotted curve. Both calculated curves are corrected for the energy dependent penetrability by Eq. 9, 10.

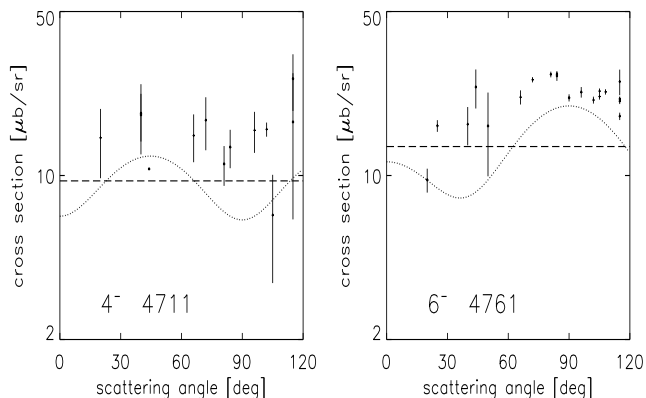


FIG. 6: Angular distributions for the  $i_{11/2}f_{5/2}$  states with spins  $7^-$ ,  $8^-$ . For the 4918 state [12] measured an excitation function at a scattering angle of  $\Theta = 158^\circ$ . The cross section on top of the IAR with  $\sigma_{LJ}^{2I} = 20 \pm 2 \mu b/sr$  agrees with the value near  $\Theta = 22^\circ$  assuming symmetry around  $\Theta = 90^\circ$ . For other details see Fig. 5.

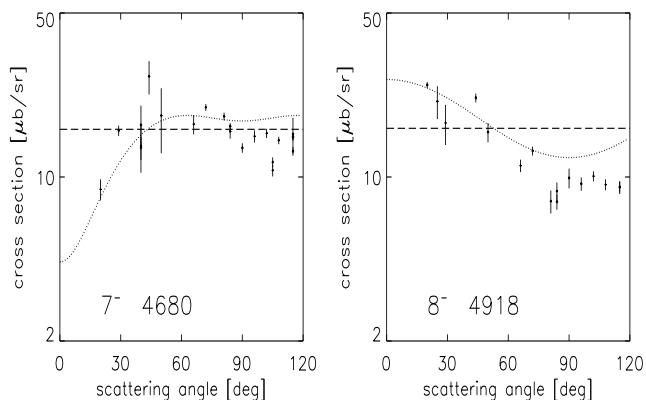
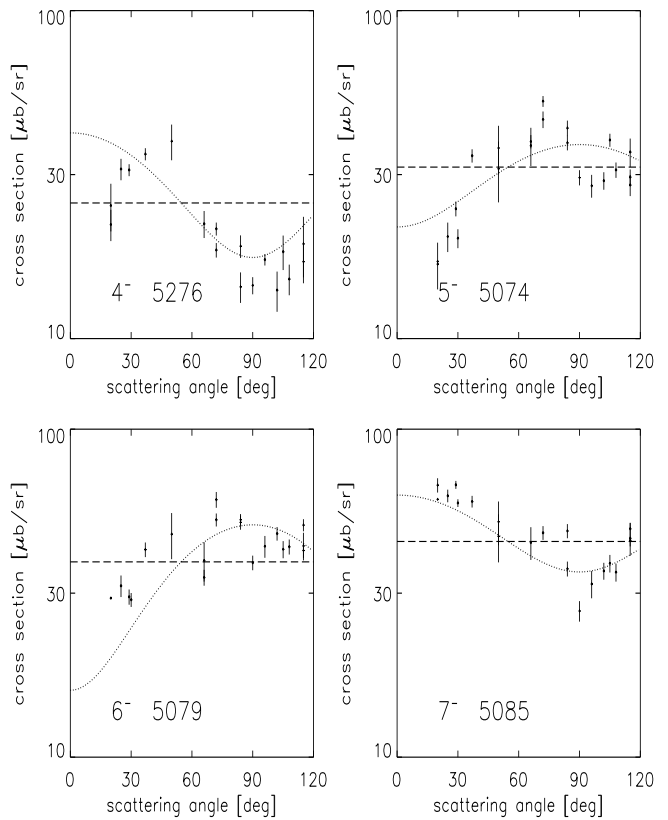


FIG. 7: Angular distributions states for the  $i_{11/2}p_{3/2}$  states with spins  $4^-$ ,  $5^-$ ,  $6^-$ ,  $7^-$ . For details see Fig. 5.



#### D. Data from $^{207}\text{Pb}(d, p)$

Tab. VI gives the results from our  $^{207}\text{Pb}(d, p)$  measurement for the ten levels in discussion. The precision of the excitation energies is slightly better than that from the IAR-pp' measurement. This may be partly explained by satellite lines due to an atomic effect which deteriorates the  $^{208}\text{Pb}(p, p')$  but not the  $^{207}\text{Pb}(d, p)$  spectra [33]. The energy of the 5075 level with a deviation of about  $2\sigma$  from [4] agrees with the result from the IAR-pp' measurement. Some levels have a vanishing  $^{207}\text{Pb}(d, p)$  cross section, especially the 4680, 4918, 5085 keV levels.

In Tab. IV, V we add the information derived from the Q3D experiment on  $^{207}\text{Pb}(d, p)$  for the region  $4.5 \text{ MeV} < E_x < 5.3 \text{ MeV}$  for levels *not* belonging to the ten states in discussion.

## VI. RESULTS AND DISCUSSION

A key assumption of the shell model is the existence of rather pure 1-particle 1-hole excitations if the spacing of the model configurations is higher than the average matrix element of the residual interaction. We verified this assumption for multiplets excited by the weakest positive parity IAR in  $^{209}\text{Bi}$ . The extremely weak excitation of

the lowest 2-particle 2-hole states (especially the  $5239 0^+$  state) adds confidence in the shell model.

In the SSM four multiplets  $i_{11/2}p_{1/2}$ ,  $i_{11/2}f_{5/2}$ ,  $i_{11/2}p_{3/2}$ ,  $i_{11/2}f_{7/2}$  are expected to be built with the  $i_{11/2}$  particle at energies  $E_x=4.210, 4.780, 5.108, 6.550$  MeV, respectively, see Fig. 1. The goal of this paper is the identification of the  $i_{11/2}f_{5/2}$ ,  $i_{11/2}p_{3/2}$  neutron particle-hole multiplets; the states containing the major strength of the configuration  $i_{11/2}p_{1/2}$  are known [2, 4, 20], see also Tab. VII; for the  $i_{11/2}f_{7/2}$  group no measurement has been done (Tab. II).

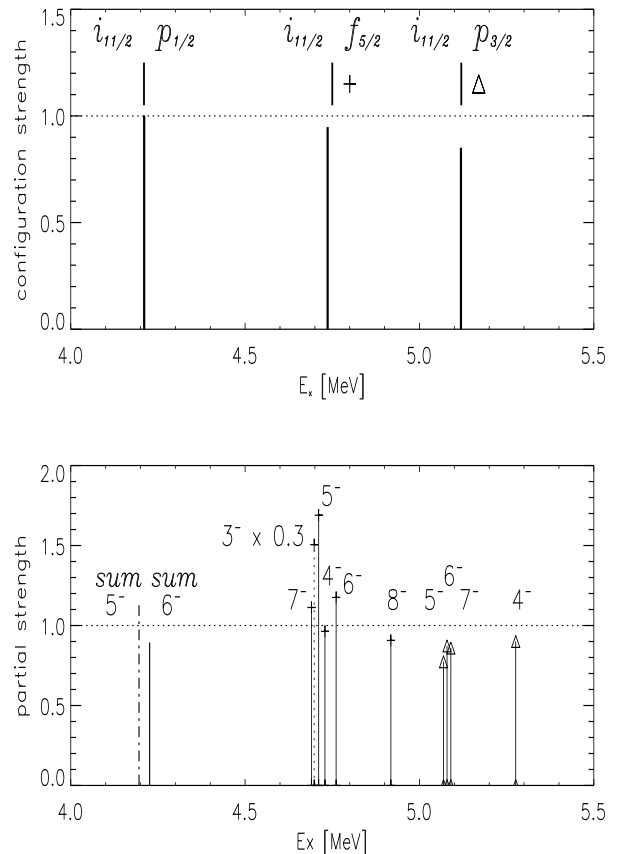
We encounter several problems with the IAR-pp' method,

- the s.p. widths  $\Gamma_{lj}^{s.p.}$  for the outgoing particles ( $lj = p_{1/2}, f_{5/2}, p_{3/2}$ ) are only known to about 10%,
- the energy dependence of the s.p. widths is rather strong and its slopes are not well known. In the region of interest a systematic error of around 20% has to be assumed,
- the mean cross section  $\sigma_{LJ}^{\alpha I}$  of a state bearing the main strength of a configuration with angular momenta  $l$  is strongly affected by the presence of a slight admixture of a configuration with lower angular momentum  $l-2$  due to the higher penetrability,
- the anisotropy of the angular distribution is highly sensitive to the mixture of the configurations. This is especially true for a small admixture of a configuration  $|lj\rangle$  with  $j = l + 1/2$  to a configuration with  $j = l - 1/2$ . In rare cases the anisotropy coefficients  $a_K/a_0$ ,  $K = 2, 4, 6, 8$  allow to determine the relative mixing of configurations  $|LJ\rangle \otimes |lj\rangle$  with  $l = 1, 3, 5$ ,  $j = l \pm 1$ .
- the angular distribution of states with natural parity often exhibit strong forward peaking via the direct-(p, p') reaction,
- the s.p. widths  $\Gamma_{i_{11/2}}^{s.p.}$ ,  $\Gamma_{j_{15/2}}^{s.p.}$  of the two weakest IAR are only known to 70%.

### A. Centroid Energy

The states strongly excited by the  $i_{11/2}$  IAR can be grouped into three parts, the first part at  $E_x \approx 4.2$  MeV belongs to the group of states strongly excited by the  $g_{9/2}$  IAR mainly, the second part at  $E_x \approx 4.6-4.8$  MeV (except for the  $4698 3^-$  state) and the third part at  $E_x \approx 5.1$  MeV are excited by no other IAR strongly. The number of states in the second and third group is six and four. (In the following discussion, the  $4698 3^-$  state is omitted since it is affected by a large direct (p, p') contribution starting at least at scattering angles  $E_x < 115^\circ$ ,

FIG. 8: In the **upper panel**, the centroid excitation energy (eq.11) and the total configuration strength  $\sum_I |c_{LJ,lj}^I|^2$  are shown. The centroid energies agree with energies  $E_x = 4.210, 4.780, 5.108$  MeV of the SSM for the three configurations  $i_{11/2}p_{1/2}$ ,  $i_{11/2}f_{5/2}$ ,  $i_{11/2}p_{3/2}$ . The total configuration strengths are close to unity using the s.p. widths from Tab. I. In the **lower panel** the excitation energies  $E_x$  and the partial strength  $|c_{LJ,lj}^I|^2$  for the states bearing the main strength of the  $p_{1/2}$ ,  $f_{5/2}$ ,  $p_{3/2}$  configurations are shown. The cross sections  $\sigma_{LJ}^{\alpha I}$  from Tab. VI are converted to partial strengths by eq.6 with s.p. widths from Tab. I and corrected for the energy dependence of the penetrability (Eq. 9, 10). For the  $i_{11/2}p_{1/2}$  multiplet the *sum* of the partial strengths of the three  $5^-$  and the three  $6^-$  states at  $4.0 \text{ MeV} < E_x < 4.5 \text{ MeV}$  is shown. The value for the  $4698 3^-$  state (left out in determining the centroid energy) is reduced by a factor 3. Both this  $3^-$  and the neighbouring  $5^-$  state are affected by the direct-(p, p') reaction yielding a much larger value than unity. The SSM expects a value  $|c_{LJ,lj}^I|^2 = 1$  (dotted line).



the maximum angle for the Q3D magnetic spectrograph in the current shape.)

We derive the centroid energies from the excitation energies  $E_x$  and the angle averaged (mean) cross sections  $\sigma_{LJ}^{\alpha I}$  of the remaining five and four states given in Tab. VI. First, we correct the mean experimental cross sections by the large change of the penetrability for the outgoing

particles across the range of excitation energies,

$$\tilde{\sigma}_{LJ}^{\alpha I} = p^2(E_x^{\alpha I}(LJ))\sigma_{LJ}^{\alpha I}. \quad (9)$$

The energy dependence of the penetrability is calculated [25] and can be linearly approximated by

$$p(E_x^{\alpha I}(LJ)) = 1 + 3.5 \frac{E_x^{\alpha I}(LJ) - E_{LJ,lj}^{SSM}}{E_{LJ,lj}^{SSM}}. \quad (10)$$

The approximation is reasonable near the SSM excitation energy of the particle-hole configurations  $|LJ\rangle \otimes |lj\rangle$  for all relevant values of  $lj$ . (The slope varies between 2.0 and 6.0 for  $8\text{ MeV} < E_{p'} < 14\text{ MeV}$  and  $l = 1, 3, 5$ , for higher  $l$ -values the slope always becoming steeper.)

We then calculate the centroid energy by the weighted mean

$$\langle E_x(LJ) \rangle = \sum_{\alpha I} \tilde{\sigma}_{LJ}^{\alpha I} E_x^{\alpha I}(LJ) \quad (11)$$

Fig. 8 *upper panel* shows the centroid energies; clearly they coincide with the prediction of the SSM model. We note that the adjustment of the s.p. widths discussed in appendix C does not affect the values of the centroid energies much.

The ratio of the sum of the angle averaged (mean) cross sections  $\tilde{\sigma}_{LJ}^{\alpha I}$  (converted to configuration strengths by use of Eq. 6) for the groups related to the  $p_{1/2}$ ,  $f_{5/2}$ ,  $p_{3/2}$ -particle compares well with the calculated ratio derived from the s.p. widths of Tab. I. We note that the shown deviations of the configuration strengths from unity are already lessened by improved s.p. widths as discussed in appendix C; using the values from [12, 14] the deviations are larger, but still in the range 10-30%.

Both the agreement of the centroid energies and the approximate agreement of the configuration strengths with the SSM expectation favour the identification of the states shown in fig. 2-8 and Tab. VI as the members of the  $i_{11/2}f_{5/2}$  and  $i_{11/2}p_{3/2}$  multiplets.

## B. Proton particle-hole configurations

IAR-pp' is sensitive to neutron particle-hole configurations only (Eq. 3). Yet with robust values of the s.p. widths and reasonable functions for the energy dependence of the penetrability, a missing configuration strength can be determined. In case the unitarity of the truncated configuration space can be trusted, by this means even amplitudes of proton particle-hole configurations can be determined. An example is give in appendix A.

The configurations  $f_{7/2}s_{1/2}$ ,  $i_{11/2}p_{3/2}$  have similar SSM energies 5.011, 5.108 MeV, respectively, including the Coulomb shift  $\Delta_C = -0.30 \pm 0.02\text{ MeV}$  (appendix A). Hence an admixture of the proton particle-hole configuration  $f_{7/2}s_{1/2}$  to the neutron particle-hole multiplet can be expected for the state with spin  $4^-$  at  $E_x=5.276\text{ MeV}$ .

It does not change the angular distribution of IAR-pp', but reduces the mean cross section only. We derive an upper limit of 20% for the  $f_{7/2}s_{1/2}$  component.

Similarly the configuration  $f_{7/2}d_{3/2}$  with the SSM energy 5.462 MeV may change the structure of the states with a dominant  $i_{11/2}p_{3/2}$  configuration. Evidently the states with spins  $6^-, 7^-$  are not affected due to the high spin; for the states with spins  $4^-, 5^-$  we derive upper limits of 20% for the  $f_{7/2}d_{3/2}$  component.

The principle of unitarity for a rather complete set of shell model configurations can be used to predict one  $4^-$  states with dominant configuration  $f_{7/2}s_{1/2}$  in the region  $E_x = 5.0 \pm 0.2\text{ MeV}$  as has been done successfully for the N=82 nucleus  $^{140}\text{Ce}$  [24, 34]. Several candidates can be found (Tab. IV, V). They should be weak on all IAR eventually except for the  $i_{11/2}$  IAR and have weak  $^{207}\text{Pb}(d, p)$  and vanishing  $^{209}\text{Bi}(d, ^3\text{He})$  cross sections.

## C. The $i_{11/2}p_{1/2}$ particle-hole multiplet

The  $i_{11/2}p_{1/2}$  strength for spin  $5^-$  is split up into three fractions, whereas the  $6^-$  strength is contained in one state mainly. The lowest  $6^-$  state at  $E_x=3919\text{ keV}$  contains less than 1% of the  $i_{11/2}p_{1/2}$  strength as shown especially by the absence of a detectable  $^{207}\text{Pb}(d, p)$  cross section both with the Buechner and the Q3D experiment. The centroid energies agree well with the prediction by the SSM model, see Fig. 8. The ratio of the total strength for the  $5^-$  and  $6^-$  states does not relate as expected from the SSM as 11:13. This hints to a considerable part of the  $i_{11/2}p_{1/2}$  strength in a higher  $6^-$  state.

Pure  $i_{11/2}p_{1/2}$  states should have isotropic angular distributions, but all six angular distributions deviate from isotropy. Small admixtures of other configurations like  $i_{11/2}f_{5/2}$ ,  $i_{11/2}p_{3/2}$ ,  $i_{11/2}f_{7/2}$  may explain the anisotropy.

For the fit shown in appendix A only few data for the configuration  $i_{11/2}p_{1/2}$  were used, namely the 4206 state to bear the overwhelming strength and and a roughly equal partition of the  $i_{11/2}p_{1/2}$   $5^-$  strength into the 4125, 4180, 4296 states. The mean cross sections now determined more precisely are in general agreement with the fit. It thus gives confidence into the fitting procedure.

The 4206 state has been already identified by [12] and used to determine the total width of the  $i_{11/2}$  IAR, see Tab. I.

## D. The $i_{11/2}f_{5/2}$ particle-hole multiplet

Tab. VI (upper part) gives the mean cross section for the states containing the major part of the  $i_{11/2}f_{5/2}$  configuration, see also Fig. 8. The states at 4680, 4698, 4709, 4711, 4761 keV have rather firm spin assignments with spins  $7^-, 3^-, 5^-, 4^-, 6^-$  according to [4]. These states – except for the  $3^-$  state at  $E_x=4698\text{ keV}$  again – have an angular distribution which can be explained by a rather pure  $i_{11/2}f_{5/2}$  configuration, see Fig. 5, 6.

We approximated the angular distribution by calculations for the pure configuration with a common factor. According to the theory [24] this factor is described by the total width  $\Gamma_{i_{11/2}}^{tot}$  which has been measured by [12] and the s.p. widths  $\Gamma_{i_{11/2}}^{s.p.}$ ,  $\Gamma_{f_{5/2}}^{s.p.}$ ,  $\Gamma_{p_{3/2}}^{s.p.}$  determined by [14]; the energy dependence is calculated [25]. In total the systematic uncertainty is about 20%. We used the adjusted values for the s.p. widths (Tab. I). We remark that the determination of the s.p. widths is complicated since they can be determined only as the product  $\Gamma_{LJ}^{s.p.}$  for the IAR and  $\Gamma_{lj}^{s.p.}$  for the outgoing particles, see Eq. 4; in addition the energy dependence of the penetrabilities is not well known.

Since the states with the main configuration  $i_{11/2}f_{5/2}$  and spins  $4^-$ ,  $5^-$ ,  $6^-$ ,  $7^-$  may mix with the configurations  $i_{11/2}p_{3/2}$  which have a much larger s.p. width  $\Gamma^{s.p.}$  due to the  $l=1$  wave instead of  $l=3$ , even a small admixture changes the angular distribution much. Seemingly this is the case for the  $4^-$ ,  $6^-$  states at  $E_x=4711$ ,  $4761$  keV, respectively, see Fig. 5, 6, hence the sum of the mean cross section according to Eq. 6 is larger than unity.

(a)  $4918$   $8^-$ . The state at  $E_x=4918$  keV is excited by the  $i_{11/2}$  IAR solely. A detection on the  $j_{15/2}$  and  $d_{5/2}$  IAR yields cross sections a factor 10 lower, see Fig. 4. The  $^{207}\text{Pb}(d, p)$  cross section is vanishing small, see Tab. VI. The agreement of the angular distribution with the calculation for a pure  $i_{11/2}f_{5/2}$  configuration is remarkable, see Fig. 6. The slight deviation may be interpreted by an admixture of the configuration  $i_{11/2}f_{7/2}$ . The absence of a sizable excitation by any other IAR corroborates the spin assignment.

At a scattering angle of  $158^\circ$ , the resonance is rising by a factor 18.0 over the direct background [12]. This fact corroborates the assignment of an unnatural parity.

(b)  $4680$   $7^-$ . The angular distribution agrees with a pure  $i_{11/2}f_{5/2}$  configuration; the slight deviation may be explained by an admixture of  $i_{11/2}f_{7/2}$ .

(c)  $4711$   $4^-$ . A weak  $i_{11/2}p_{3/2}$  admixture explains the augmented cross section (Fig. 5) by the much higher penetrability of the  $p_{3/2}$  particle. A weak excitation by the  $^{207}\text{Pb}(d, p)$  reaction is consistent with a sizeable excitation by the  $g_{9/2}$  IAR (Fig. 4).

(d)  $4761$   $6^-$ . A fraction of about 10% of the  $6^-$   $i_{11/2}p_{1/2}$  strength in the 4761 keV state relieves both the augmented mean cross section (Fig. 6) and the discrepancy found while discussing the  $i_{11/2}p_{1/2}$  strength above. It is consistent with the detected  $^{207}\text{Pb}(d, p)$  reaction; both the Buechner and the Q3D data can be explained by a  $0.10 \pm 0.04$   $i_{11/2}p_{1/2}$  admixture.

(e)  $4709$   $5^-$ . The deviation of the angular distribution at forward angles can be explained by a direct-(p, p') component; it is consistent with the assignment of natural parity. Seemingly an admixture of  $g_{9/2}p_{1/2}$  or  $i_{11/2}p_{1/2}$  is small; it is consistent with the smaller cross section for  $^{207}\text{Pb}(d, p)$  in relation to the 4711 doublet member.

(f)  $4698$   $3^-$ . The 4698  $3^-$  state is excited at forward

angles ten times stronger as predicted by the SSM, but from the excitation functions of ref.[13] we derive upper limits for the backward angles  $150^\circ$ ,  $170^\circ$  which are consistent with the pure  $i_{11/2}f_{5/2}$  configuration in contrast to the forward angles symmetric to  $90^\circ$ . The state is also known to have sizable  $g_{9/2}p_{3/2}$  and  $d_{5/2}p_{1/2}$  components [20]. The excitation by the  $^{207}\text{Pb}(d, p)$  reaction is consistent with a rather strong  $d_{5/2}p_{1/2}$  component.

A possible alimentionation on top of the  $i_{11/2}$  IAR via the exit channel  $d_{5/2}p_{1/2}$  may change the angular distribution due to the higher penetrability of the outgoing  $p_{1/2}$  particle. The rather strong direct-(p, p') component contributes in addition. Therefore the interpretation of this state is complicate.

The angular distribution for the 4.70 MeV level shown by [12, 13] is interpreted incorrectly by the authors. Namely the resolution of about 35 keV was insufficient to resolve this state from the neighbouring multiplet at 4680, 4709, 4711 keV. So the strong excitation by the  $i_{11/2}$  IAR is not due to the excitation of the  $3^-$  state alone, but at least equally to the  $7^-$ ,  $5^-$ ,  $4^-$  multiplet around it. So the surprise about the strong excitation of the "4.692 MeV" level [14] is solved.

### E. The $i_{11/2}p_{3/2}$ particle-hole multiplet

The angular distributions of the four states containing most of the  $i_{11/2}p_{3/2}$  strength is shown in Fig. 7. Calculations for spins  $4^-$ ,  $5^-$ ,  $6^-$ ,  $7^-$  are inserted. Tab. VI (lower part) gives the mean cross section for the triplet levels at 5075, 5079, 5085 and the 5276 level. Comparing the cross sections for the resolved triplet levels at  $\Theta = 90^\circ, 22^\circ$  to the data points at  $\Theta = 90^\circ, 158^\circ$  (ie. symmetric to  $90^\circ$ ) from the excitation function of the 5.071 MeV level unresolved by [12] we find agreement within 10%. This shows that the direct-(p, p') contribution is low.

(a)  $5085$   $7^-$ . The 5085 state is assumed to have spin  $7^-$  [4]. Its angular distribution is well fitted by assuming a pure  $i_{11/2}p_{3/2}$  configuration and very similar to that from the  $i_{11/2}f_{5/2}$  configuration with the highest spin  $I = J + j$ . A preliminary analysis of more data designates the  $8^-$  member of the  $g_{9/2}f_{7/2}$  multiplet as a state at  $E_x=5936$  keV. It exhibits a similar steep rise of the angular distribution towards forward angles indicating a rather pure neutron particle-hole configuration with spin  $I = J + j$ , too.

(b)  $5075$   $5^-$ ,  $5079$   $6^-$ . The 5075, 5079 states of the triplet are assigned spin  $5^-$ ,  $6^-$ . A reverse spin assignment fits worse, since the mean cross section of the 5079 level is about 20% higher, see Tab. VI. The 5075 and 5085 states are excited sizable on both the  $d_{5/2}$  and  $s_{1/2}$  IAR (the 5085 state also on the  $d_{3/2}+g_{7/2}$  doublet IAR). This may be due to a considerable direct-(p, p') cross sections and corroborates the assignment of natural parity spins in contrast to the low cross section of the 5079 state on all other IAR, see Fig. 4.

In the excitation functions for the scattering angles  $90^\circ, 158^\circ$  the cross section is rising by a factor 10.0, 13.7 over the direct background, respectively. This fact may hint to a small contribution from direct-(p, p') for the  $7^-$  state.

(c)  $5276\ 4^-$ . The missing  $4^-$  member is identified as the 5276 keV state. It is strongly excited by the  $i_{11/2}$  IAR, but only weakly on all other IAR, see Fig. 4. The angular distribution is well described by a pure  $i_{11/2}p_{3/2}$  configuration, see Fig. 7. The cross section is somewhat higher than expected, see Fig. 6. Only a complete fit of all levels participating in the configuration mixing with  $|g_{9/2} \otimes |lj \rangle$  and  $|i_{11/2} \otimes |lj \rangle$  and another readjustment of

the s.p. widths will solve the problem.

(d) *Information from  $^{207}\text{Pb}(d, p)$ .* The  $4680\ 7^-$ ,  $4918\ 8^-$ ,  $5085\ 7^-$  states have vanishing  $^{207}\text{Pb}(d, p)$  cross sections corroborating the spin and configuration assignments. We explain the excitation by the  $^{207}\text{Pb}(d, p)$  reaction for the  $5075\ 5^-$  state by a weak  $i_{11/2}p_{1/2}$  admixture, for the  $5079\ 6^-$  state by a weak  $i_{11/2}p_{1/2}$  admixture, for the  $5276\ 4^-$  state by a weak  $g_{7/2}p_{1/2}$  admixture. The  $g_{7/2}p_{1/2}$  admixture of the  $5276\ 4^-$  state is corroborated by the excitation on the  $d_{3/2}+g_{7/2}$  doublet IAR, see Fig. 4.

TABLE VI: Energies, spins and cross sections for the ten states in the range  $4.6\ \text{MeV} < E_x < 5.3\ \text{MeV}$  discussed in the text with configurations  $i_{11/2}f_{5/2}$  (upper part),  $i_{11/2}p_{3/2}$  (lower part). The energies and the mean cross sections  $\sigma_{LJ}^{\alpha I}$  are determined from the  $^{208}\text{Pb}(p, p')$  experiment. The cross sections  $\tilde{\sigma}_{LJ}^{\alpha I}$  on top of the  $i_{11/2}$  IAR are corrected for the energy dependence of the penetrability by Eq. 9, the cross sections on top of the  $g_{9/2}, d_{5/2}$  IAR are reduced by the penetrability ratio  $R_{g_{9/2}}, R_{d_{5/2}}=8, 12$  (Eq. 7). Cross sections for pure  $i_{11/2}f_{5/2}$  and  $i_{11/2}p_{3/2}$  configurations are calculated from Eq. 6 with  $|c_{i_{11/2}f_{5/2}}|^2 = 1$  respectively  $|c_{i_{11/2}p_{3/2}}|^2 = 1$  using s.p. widths from Tab. I (col. 11). From  $^{207}\text{Pb}(d, p)$  performed with the Q3D facility, energies (col. 2) and cross sections  $\sigma(\approx 25^\circ)$  are derived, too. Spins from [4] and energies from [2, 3, 4] are given for comparison.

$E_x$ keV (p, p')	$E_x$ keV (d, p)	spin	spin	$E_x$ keV	$E_x$ keV	$E_x$ keV	$\sigma(25^\circ)$ $\mu\text{b}/\text{sr}$ (d, p)	$\sigma_{LJ}^{\alpha I}/R_{LJ}$ $\mu\text{b}/\text{sr}$ (p, p')	$\tilde{\sigma}_{LJ}^{\alpha I}$ $\mu\text{b}/\text{sr}$ (p, p')	$\sigma_{LJ}^{\alpha I}$ $\mu\text{b}/\text{sr}$ (p, p')	$\sigma_{LJ}^{\alpha I}/R_{LJ}$ $\mu\text{b}/\text{sr}$ (p, p')	remark
								on $g_{9/2}$	on $i_{11/2}$	on $i_{11/2}$	on $d_{5/2}$	
(a)	(a)	(a)	[4]	[2]	[4]	[3]	(a)	(a)	(a)	calcul.	(a)	(a) this work
4680.3 $\pm 0.5$	-	$7^-$	( $7^-$ )	4680.7 $\pm 0.5$	4680.310 $\pm 0.250$	-	$< 2$	0.2	16	16.2	0.3	
4698.5 $\pm 0.3$	4698.40 $\pm 0.15$	$3^-$	$3^-$	4698.4 $\pm 0.5$	4698.375 $\pm 0.040$	4697.9 $\pm 0.1$	800	1.2	45 (b)	6.6	1.6	(b) see text
4709.4 $\pm 0.8$	-	$5^-$	( $5^-$ )	4709.5 $\pm 3.5$	4709.409 $\pm 0.250$	-	10	1.7	11	10.5	1.4	
4711.2 $\pm 0.8$	4711.0 $\pm 0.6$	$4^-$	$4^-$	-	4711.300 $\pm 0.750$	-	15	0.5	15	8.6	0.9	
4761.9 $\pm 0.5$	4762.1 $\pm 0.4$	$6^-$	$6^-$	4761.8 $\pm 0.5$	4761.800 $\pm 0.250$	-	7	0.5	19	12.4	0.3	
4918.8 $\pm 0.4$	-	$8^-$	-	4917.6 $\pm 1.5$	-	-	$< 2$	0.1	15	16.2 (c)	0.2	(c) adapted, see text
5074.6 $\pm .5$	5074.8 $\pm 0.4$	$5^-$	-	5073.7 $\pm 1.5$	5075.800 $\pm 0.200$	-	9	0.6	32	34	0.9	
5079.8 $\pm .6$	5079.8 $\pm 0.7$	$6^-$	-	-	-	-	5	0.5	40	40	0.5	
5085.3 $\pm .4$	-	$7^-$	( $7^-$ )	5084.7 $\pm 1.5$	5085.550 $\pm 0.250$	5085.7 $\pm 0.2$	$< 2$	0.5	46	46 (d)	1.0	(d) adapted, see text
5276.4 $\pm .5$	5276.2 $\pm 0.2$	$4^-$	-	5277.1 $\pm 1.5$	-	-	70	0.3	26	27	0.5	

## VII. CONCLUSION

The shell model is verified to explain the structure of 30 negative parity states in  $^{208}\text{Pb}$  below  $E_x=5.3\ \text{MeV}$  by 1-

particle 1-hole configurations, 10 states more than in the first derivation of matrix elements of the residual interaction by [20]. The states containing the major strength of the configuration  $i_{11/2}p_{1/2}$  were measured. Amplitudes

of the configuration  $i_{11/2}p_{1/2}$  obtained by an update of the fit done by [20] are verified to be approximately correct, see appendix A.

The ten states containing the major strength of the multiplets  $i_{11/2}f_{5/2}$  and  $i_{11/2}p_{3/2}$  are identified. All states have one dominant shell model neutron particle-hole configuration except for the  $i_{11/2}f_{5/2}$  member with the lowest spin  $3^-$ . Some minor admixtures of other configurations derived from the analysis of  $^{208}\text{Pb}(p, p')$  are consistent with results from  $^{207}\text{Pb}(d, p)$ . The detection of the members with the highest spins from the  $i_{11/2}f_{5/2}$  and  $i_{11/2}p_{3/2}$  group (and of  $g_{9/2}f_{7/2}$ , too) gives hope to find even the  $i_{11/2}f_{7/2}$  group members with spins  $8^-$  and  $9^-$  expected at an energy  $E_x = 6.550$  MeV which might be rather pure.

The clear identification of the  $i_{11/2}f_{5/2}$  and  $i_{11/2}p_{3/2}$  group and the more carefully measured angular distributions of the states containing  $i_{11/2}p_{1/2}$  strength

will help to refine the derivation of a more complete shell model transition matrix extending the configuration space up to  $E_x \approx 5.2$  MeV similar as done by [20], at least for the higher spins. Admixtures of proton particle-hole configurations can be obtained in principle by the assumption of a rather complete subshell closure and the observation of the ortho-normality rule and sum-rule relations; this fact becomes more relevant since for the higher proton particle-hole configurations there is no target for transfer reactions of the type  $^{209}\text{Bi}(d, ^3\text{He})$ .

The goal to determine of matrix elements of the effective residual interaction among particle-hole configurations in  $^{208}\text{Pb}$  can be approached better than done by [20] due to the higher quality and larger amount of experimental data. The evaluation of existing data from our measurements of  $^{208}\text{Pb}(p, p')$  and  $^{207}\text{Pb}(d, p)$  will allow to extend the configuration space up to eventually  $E_x \approx 6.1$  MeV.

TABLE VII: Update of the fit from [20]: Unitary transformation  $||c_{LJ,lj}^{\alpha I,(\nu,\pi)}||$  of the shell model particle-hole configurations below  $E_x = 4.5$  MeV to the states  $|\alpha I \rangle$  with spins  $4^-, 5^-, 6^-$ . The errors of the amplitudes are of the order of 0.01 for amplitudes close to  $|c| = 1$  and up to 0.20 for  $|c| \approx 0$ . *Footnote: (a)* A sizable admixture in the order of about  $|c| = 0.1$  of  $g_{9/2}h_{9/2}$  and  $g_{9/2}h_{11/2}$  is needed to fit the angular distribution; it depends on the component  $a_8$  from the fit of the angular distribution by  $d\sigma(\Theta)/d\Omega = \sum_K^{0,2,4,6,8} a_K P_K(\cos(\Theta))$ .

$E_x(\text{keV})$	spin	$g_{9/2}p_{1/2}$	$g_{9/2}f_{5/2}$	$g_{9/2}p_{3/2}$	$g_{9/2}f_{7/2}$	$i_{11/2}p_{1/2}$	$h_{9/2}s_{1/2}$	$h_{9/2}d_{3/2}$
3475	$4^-$	+ .985	+ .060	- .280	- .013		+ .050	- .176
3946	$4^-$	- .050	+ .293	- .030	.000		+ .937	+ .118
3995	$4^-$	- .110	+ .984	- .065	.000		- .389	+ .018
4262	$4^-$	+ .050	+ .070	+ .569	.000		+ .182	+ .559
4383	$4^-$	.000	+ .037	+ .863	.000		+ .100	- .349
3192	$5^-$	+ .780	+ .350	+ .220	- .100	- .150	- .230	+ .170
3709	$5^-$	- .430	+ .491	- .130	.000	- .300	- .520	+ .400
3960	$5^-$	- .010	+ .690	.000	.000	.000	+ .720	.000
4125	$5^-$	- .050	- .340	+ .270	.000	- .440	+ .330	+ .610
4180	$5^-$	.000	+ .015	+ .590	.000	+ .720	- .130	+ .250
4292	$5^-$	- .050	+ .150	+ .620	.000	- .400	- .100	- .600
3919 <sup>a</sup>	$6^-$		+ .981	- .062	+ .119	+ .110		+ .137
4206	$6^-$		- .222	+ .045	- .010	+ .960		- .326
4383	$6^-$		- .207	- .338	.000	+ .235		+ .900
4480	$6^-$		- .083	+ .905	- .032	+ .231		+ .401

#### APPENDIX A: UPDATE OF THE FIT OF STATES IN $^{208}\text{PB}$ BELOW $E_x=4.5$ MEV FROM IAR-PP' DATA

Tab. VII presents the update of the fit shown in [20] using the same data base, namely angular distribution measurements of  $^{208}\text{Pb}(p, p')$  near the  $g_{9/2}$  IAR [35] (see also an edited version in [28]),  $^{207}\text{Pb}(d, p)$  data from the Buechner experiment as described in the text, and other data from [5], but in addition data from the  $^{209}\text{Bi}(d, ^3\text{He})$  experiment [21] done in 1981.

The results for spins  $2^-, 3^-, 7^-$  are only slightly

changed by a readjustment of the s.p. widths and therefore not shown here. The errors are not shown, but of the order of 0.01 for amplitudes close to  $|c| = 1$  up to 0.20 for  $|c| \approx 0$ . The detailed discussion is complicated, but foreseen to be done in a future publication. The errors are similar to those in [20] since the data base is identical except for the new  $^{209}\text{Bi}(d, ^3\text{He})$  data. The essential difference of the update from [20] consists only in a few other state identifications and some interchanged spin assignments.

The centroid energies derived from this fit agree well with the predictions of the SSM (Tab. VIII). For the

proton particle-hole configurations we derive a Coulomb shift of  $\Delta_C = -0.30 \pm .02 \text{ MeV}$ .

## APPENDIX B: $W$ -, $\bar{Z}$ - AND ANISOTROPY COEFFICIENTS

For the programming of Eq. 4 in modern computer languages we give the definition of the  $W$ - and  $\bar{Z}$ -coefficients in terms of 3j- and 6j-symbols. The  $W$ -coefficient is derived from the 6j-symbol as [26, 27]

$$W(j_1 j_2 l_2 l_1; j_3 l_3) = (-1)^{j_1 + j_2 + l_2 + l_1} \left\{ \begin{matrix} j_1 j_2 j_3 \\ l_1 l_2 l_3 \end{matrix} \right\}. \quad (\text{B1})$$

The  $\bar{Z}$ -coefficient is converted from the definition by [26, 27] with  $W$ - and Clebsch-Gordon coefficients as

$$\bar{Z}(abcd; ef) = \sqrt{(2a+1)(2b+1)(2c+1)(2d+1)} (-1)^{a-c} \sqrt{2f+1} \begin{pmatrix} acf \\ 000 \end{pmatrix} \left\{ \begin{matrix} abe \\ def \end{matrix} \right\} i^{f-a+c}. \quad (\text{B2})$$

Examples of the anisotropy coefficients  $a_K/a_0$  for pure particle-hole configurations  $|LJ\rangle \otimes |lj\rangle$  calculated from Eq.6 are shown in Fig. 9. They vary in a systematic manner with the angular momentum and spin of the particle  $LJ$  and the hole  $lj$ . For the lowest and highest spin  $I = J \pm j$  the angular distribution has a deep minimum at  $\Theta = 90^\circ$  as can be derived from the values of the anisotropy coefficients  $a_K/a_0$ .

FIG. 9: Anisotropy coefficients  $a_2/a_0, a_4/a_0$ , of the angular distribution for the particle-hole configurations  $|LJ\rangle \otimes |lj\rangle$  with a  $g_{9/2}, i_{11/2}, j_{15/2}$  particle coupled to a  $f_{5/2}$  hole. The values are connected from the lowest to the highest spin  $I = J \pm j$ . The configuration  $i_{11/2}p_{3/2}$  with spins  $I^\pi = 4^-, 5^-, 6^-, 7^-$  (marked explicitly) has  $a_4 = 0$ .

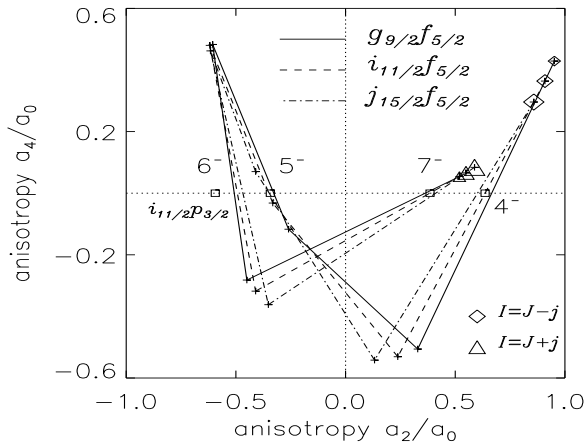


TABLE VIII: Centroid energies derived from the fit (Tab. VII).

	$g_{9/2}p_{1/2}$ MeV	$g_{9/2}f_{5/2}$ MeV	$g_{9/2}p_{3/2}$ MeV	$i_{11/2}p_{1/2}$ MeV	$h_{9/2}s_{1/2}$ MeV	$h_{9/2}d_{3/2}$ MeV
SSM	3.41	3.98	4.31	4.21	4.21	4.56
fit	3.40	3.93	4.32	4.18	3.92	4.25

## APPENDIX C: IMPROVED S.P. WIDTHS

The values of the s.p. widths  $\Gamma_{LJ}^{s.p.}$  for the IAR  $LJ$  in Tab. I were derived by [12] from the analysis of the excitation functions. The values of the s.p. widths  $\Gamma_{lj}^{s.p.}$  for the outgoing particles  $lj$  were derived by [14]. They divided the levels below  $E_x \approx 4.5 \text{ MeV}$  excited strongly by the  $g_{9/2}$  IAR into three groups assigned to bear the main strength of the configurations  $g_{9/2}p_{1/2}, g_{9/2}f_{5/2}, g_{9/2}p_{3/2}$ . This is good to first approximation (see Tab. VII in the appendix A). As we have detected similar groups for the  $i_{11/2}$  IAR we can improve the values.

Using the s.p. widths  $\Gamma_{lj}^{s.p.}$  from Tab. I, the comparison of the mean cross sections for the states  $E_x < 4.5 \text{ MeV}$  mainly excited by the  $g_{9/2}$  IAR to the states  $4.5 \text{ MeV} < E_x < 5.3 \text{ MeV}$  almost solely excited by the  $i_{11/2}$  IAR allows to derive an improved value of  $\Gamma_{i_{11/2}}^{s.p.}$ . We find a value of  $2.2 \text{ keV}$  with an error of about 10%, an improvement from [12, 14] by a factor 5.

More precise values of  $\Gamma_{lj}^{s.p.}$  can be derived by considering states which contain essentially only one SSM configuration. With the  $g_{9/2}$  particle there are four states, with the  $i_{11/2}$  particle there are six states; in addition the sum of the configuration strength for the  $i_{11/2}p_{1/2}$  configuration is known due to the analysis of [20] (see Tab. VII) together with our new Q3D data.

The lowest  $4^-$  state at  $E_x = 3.475 \text{ MeV}$  is a rather pure  $g_{9/2}p_{1/2}$  configuration with a considerable  $g_{9/2}p_{3/2}$  admixture [9] and less than 1% admixture from  $g_{9/2}f_{5/2}, g_{9/2}f_{7/2}$ , see Tab. VII. The 4480  $6^-$  state bears the main part of  $g_{9/2}p_{3/2}$  configuration with about 20% admixture from other configurations not related to the  $g_{9/2}$  IAR. The 3919  $6^-$  state bears the main part of  $g_{9/2}f_{5/2}$  configuration with about 1% admixture of  $g_{9/2}p_{3/2}$ ; similarly the 3995  $4^-$  state bears the main part of  $g_{9/2}f_{5/2}$  configuration with 1.5% admixture from  $g_{9/2}p_{1/2}, g_{9/2}p_{3/2}$ . Due to the much higher penetrability of the  $l = 1$  particle in relation to the  $l = 3$  particle, in effect the 1-2% admixture changes the mean cross section by about 15%.

Fig. 8 shows the partial strength for the ten states with a  $i_{11/2}f_{5/2}$  or  $i_{11/2}p_{3/2}$  component in the upper panel. The sum of the values for the states with spins  $5^-, 6^-$  bearing the essential  $i_{11/2}p_{1/2}$  strength are shown, too.

We adjusted the s.p. widths  $\Gamma_{lj}^{s.p.}$  thus that a unitarity close to unity is obtained simultaneously for the above mentioned states strongly excited by the  $g_{9/2}$  IAR (3475, 3919, 3995, 4480), and the states strongly excited by the  $i_{11/2}$  IAR. Here we excepted the states 4698, 4709, 4711,

4760 (see discussion below) and included the sum of the  $i_{11/2}p_{1/2}$  configuration strength obtained.

The systematic error in the absolute cross sections is around 10%, so we stick to the value  $\Gamma_{p_{1/2}}^{s.p.}$  given by [12], but derive a slightly lower value  $\Gamma_{p_{3/2}}^{s.p.}=14.6$  keV at an energy  $E_{p'}=10.59$  MeV, and a considerable higher value

$\Gamma_{f_{5/2}}^{s.p.}=5.2$  keV at an energy  $E_{p'}=10.92$  MeV, see Tab. I.

*Other s.p. widths.* From a preliminary analysis of some states, in relation to other IAR rather strongly excited on the  $j_{15/2}$ ,  $g_{9/2}$  IAR, we derive values for  $\Gamma_{j_{15/2}}^{s.p.}$ ,  $\Gamma_{f_{7/2}}^{s.p.}$  in a similar manner (Tab. I).

- 
- [1] Minfang Yeh, P. E. Garrett, C. A. McGrath, S. W. Yates, and T. Belgya. *Phys. Rev. Lett.*, 76:1208, (1996).
- [2] B. D. Valnion, V. Yu. Ponomarev, Y. Eisermann, A. Gollwitzer, R. Hertenberger, A. Metz, P. Schiemenz, and G. Graw. *Phys. Rev.*, C63:024318, (2001).
- [3] E. Radermacher, M. Wilhelm, S. Albers, J. Eberth, N. Nicolay, H.-G. Thomas, H. Tiesler, P. von Brentano, R. Schwengner, S. Skoda, G. Winter, and K. H. Maier. *Nucl. Phys.*, A597:408, (1996).
- [4] M. Schramm, K. H. Maier, M. Rejmund, L. D. Wood, N. Roy, A. Kuhnert, A. Aprahamian, J. Becker, M. Brinkman, D. J. Decman, E. A. Henry, R. Hoff, D. Mantatt, L. G. Mann, R. A. Meyer, W. Stoeffl, G. L. Struble, T.-F. Wang. *Phys. Rev.*, C56:1320, (1997).
- [5] M. B. Lewis. *Nucl. Data Sheets*, 5:243, (1971).
- [6] M. J. Martin. *Nucl. Data Sheets*, 47:797, (1986).
- [7] C. F. Moore, J. G. Kulleck, P. von Brentano, F. Rickey. *Phys. Rev.*, 164:1559, (1967).
- [8] P. Richard, W. G. Weitkamp, W. Wharton, H. Wieman, P. von Brentano. *Phys. Lett.*, 26B:8, (1967).
- [9] J. P. Bondorf, P. von Brentano, P. Richard. *Phys. Lett.*, 27B:5, (1968).
- [10] J. G. Cramer, P. von Brentano, G. W. Phillips, H. Ejiri, S. M. Ferguson, W. J. Braithwaite. *Phys. Rev. Lett.*, 21:297, (1968).
- [11] P. von Brentano, W. K. Dawson, C. F. Moore, P. Richard, W. Wharton, H. Wieman. *Phys. Lett.*, 26B:666, (1968).
- [12] W. R. Wharton, P. von Brentano, W. K. Dawson, P. Richard. *Phys. Rev.*, 176:1424, (1968).
- [13] S. A. A. Zaidi, L. J. Parish, J. G. Kulleck, C. F. Moore, P. von Brentano. *Phys. Rev.*, 165:1312, (1968).
- [14] P. Richard, P. von Brentano, H. Wieman, W. Wharton, W.G.Weitkamp, W.W.McDonald, D.Spalding. *Phys. Rev.*, 183:1007, (1969).
- [15] J. G. Kulleck, P. Richard, D. Burch, C. F. Moore, W. R. Wharton, P. von Brentano. *Phys. Rev.*, C2:1491, (1970).
- [16] R. Hertenberger, Y. Eisermann, H.-F. Wirth, and G. Graw. Maier-Leibnitz Laboratorium, annual report. *Universität München*, page 70, (2000). [http://www.bl.physik.uni-muenchen.de/bl\\_rep/jb2000/p70.ps](http://www.bl.physik.uni-muenchen.de/bl_rep/jb2000/p70.ps).
- [17] H.-F. Wirth, H. Angerer, T. von Egidy, Y. Eisermann, G.Graw, and R.Hertenberger. Maier-Leibnitz Laboratorium, annual report. *Universität München*, page 71, (2000). [http://www.bl.physik.uni-muenchen.de/bl\\_rep/jb2000/p71.ps](http://www.bl.physik.uni-muenchen.de/bl_rep/jb2000/p71.ps).
- [18] H.-F. Wirth. Ph.D. thesis, (2001). <http://tumb1.biblio.tu-muenchen.de/publ/diss/ph/2001/wirth.html>.
- [19] R. Hertenberger, A. Metz, Y. Eisermann, K. El Abiary, A. Ludewig, C. Pertl, S. Trieb, H.-F. Wirth, P. Schiemenz, G. Graw,. *Nucl. Inst.*, A536:266, (2005).
- [20] A. Heusler and P. von Brentano. *Ann. Phys. (N.Y.)*, 75:381, (1973).
- [21] G. Mairle, K. Schindler, P. Grabmayr, G.J. Wagner, I. Schmidt-Rohr. *Phys. Lett.*, 121B:307, (1983).
- [22] M. Rejmund, M. Schramm, K. H. Maier. *Phys. Rev.*, C59:2520, (1999).
- [23] A. Bohr and Ben R. Mottelson. *Nuclear Structure*, volume I. W. A. Benjamin, New York, Amsterdam, (1969).
- [24] A. Heusler, H. L. Harney and J. P. Wurm. *Nucl. Phys.*, A135:591, (1969).
- [25] R. G. Clarkson, P. von Brentano, and H. L. Harney. *Nucl. Phys.*, A161:49, (1971).
- [26] J. M. Blatt, L. C. Biedenharn, and M. E. Rose. *Revs. Mod. Phys.*, 24:249, (1952).
- [27] A. R. Edmonds. *Angular momentum in quantum mechanics*. Princeton University Press, (1960).
- [28] A. Heusler. <http://www.mpi-hd.mpg.de/~hsl/>.
- [29] A. Heusler, M. Endriss, C. F. Moore, E. Grosse, P. von Brentano. *Z. Physik*, 227:55, (1969).
- [30] G. Latzel and H. Paetz Gen. Schieck. *Nucl. Phys.*, A323:413, (1979).
- [31] F. Riess. <http://www.cip.physik.uni-muenchen.de/~riess/>.
- [32] A. Heusler, G. Graw, R. Hertenberger, H.-F. Wirth, P. von Brentano. Maier-Leibnitz Laboratorium, annual report. *Universität München*, page 21, (2004). [http://www.bl.physik.uni-muenchen.de/bl\\_rep/jb2004/p021.ps](http://www.bl.physik.uni-muenchen.de/bl_rep/jb2004/p021.ps).
- [33] A. Heusler, G. Graw, R. Hertenberger, H.-F. Wirth, P. von Brentano. Maier-Leibnitz Laboratorium, annual report. *Universität München*, page 21, (2003). [http://www.bl.physik.uni-muenchen.de/bl\\_rep/jb2004/p21.ps](http://www.bl.physik.uni-muenchen.de/bl_rep/jb2004/p21.ps).
- [34] A. Heusler. *Nucl. Phys.*, A141:667, (1970).
- [35] H.-J. Glöckner. Master's thesis, Universität Heidelberg, (1972).